Developing a molecular-level understanding of biochar materials using public characterization data

Please cite this article in press as: Wood et al., Developing a molecular-level understanding of biochar materials using public characterization data, Cell Reports Physical Science (2024), https://doi.org/10.1016/j.xcrp.2024.102036

Cell Reports
Physical Science

CellPress
OPEN ACCESS

Perspective

Developing a molecular-level understanding of biochar materials using public characterization data

Rosie Wood,[1] Ondřej Mašek,[2] and Valentina Erastova[1,*]

SUMMARY

Biochars are black carbonaceous solids produced through biomass pyrolysis under conditions of little or no oxygen. While their properties and applications are well studied, the underlying molecular structures are poorly defined. Consequently, there has been limited computational study of biochars, despite the advantages of such techniques. In part one of this two-part study, we review the experimental techniques to characterize biochar and biochar-like materials and discuss the ambiguities, errors, and uncertainties inherent to each technique. We focus on techniques that provide chemical information and molecular-level insights, thereby adding to our understanding of the molecular structures comprising biochars. We also collect publicly available characterization data for woody biochars across a range of the highest treatment temperatures of pyrolysis. These collected data provide a quantitative description of the changes in biochar properties with increasing pyrolysis temperature. The collected data, shared as an open database, support the further development of biochar molecular models, reported in part two of this work.

INTRODUCTION

Biochars, charcoals, and chars are black carbonaceous solids produced through the pyrolysis of biomass, an organic material from previously living organisms as well as anthropogenic waste materials, under conditions of little or no oxygen. The properties of the resulting materials are incredibly variable and heavily influenced both by the starting feedstock and the conditions used during pyrolysis. This variability renders biochars suitable for diverse applications. Water decontamination, carbon capture, and soil-nutrient enhancement are but a few examples.[1]

A clear understanding of structure-property relationships within biochars is vital when attempting to identify optimal feedstocks and production conditions for a given application. This can be achieved through a series of systematic and well-thought-out experiments. However, this process is highly laborious, resource intensive, and, due to the heterogeneity of biochars, must be repeated many times to reduce uncertainties. Computational techniques, such as molecular dynamics (MD), have been gaining popularity due to their ability to describe a system's structure-property relationships. Modeling allows for systematic and reproducible investigations, testing hypotheses, and informing experiments. However, while the properties of biochars are well understood individually,[2] relatively little is known about the underlying molecular structures. As a result, realistic molecular models of

[1]School of Chemistry, University of Edinburgh, Joseph Black Building, David Brewster Road, King's Buildings, Edinburgh EH9 3FJ, UK

[2]UK Biochar Research Centre, School of GeoSciences, University of Edinburgh, Crew Building, Alexander Crum Brown Road, King's Buildings, Edinburgh EH9 3FF, UK

*Correspondence: valentina.erastova@ed.ac.uk

https://doi.org/10.1016/j.xcrp.2024.102036

biochars are virtually non-existent, drastically limiting the scope of MD study of these materials.

The goal of this work is to gain insights into the molecular structures of biochars, understand how these structures vary with production conditions, and create and distribute a set of biochar molecular models to be used in MD studies. This work is in two parts: part 1 provides insights into the molecular structures within biochars (current article), and part 2 covers the development of realistic molecular models of biochars (see Wood et al.[3] in this issue of *Cell Reports Physical Science*). We begin by setting biochars in context and with a brief discussion of feedstocks and their influence on biochar properties. We then examine the different analytical techniques used to characterize these materials along with their ambiguities, errors, and uncertainties. This allows us to assess the information gained by each technique critically. We focus predominantly on techniques that yield molecular-level insights into biochars, thereby adding to our understanding of biochars' molecular makeup. We also collect experimental data from the literature into an open database (accessible via https://github.com/Erastova-group/Biochar_MolecularModels). And finally, we use these data to gather quantitative insights into the influence of one of the most significant production parameters—the highest treatment temperature (HTT)—on the properties of biochars. We use these data to illustrate the relationships between HTT and biochar properties and, therefore, to infer the influence of HTT on molecular structure. The collected data, supported by the deeper understanding of biochars' molecular makeup, aid us in the development of a set of realistic molecular models of biochars, presented in the second part of this work.[3]

Natural and manufactured carbonaceous materials

Biochars are formed through the carbonization of organic matter during pyrolysis. As they share similar precursors (lignocellulosic biomass), it is useful to consider biochars alongside natural carbonaceous solids, such as coals and kerogens. These may be regarded as natural analogs to biochars,[4] and, as a result, many of the analytical techniques used to characterize biochars originate from the characterization of these natural materials.

Coals are defined as carbonaceous sedimentary rocks containing at least 50 wt % organic matter. They are usually formed from terrestrial biomass, such as woody organic matter.[4,5] On the other hand, kerogens are carbonaceous solids derived from sedimentary rocks containing less than 50 wt % organic matter. They are defined as being insoluble in non-oxidizing acids, bases, and organic solvents.[4] There are three main types of kerogens: types I and II, which originate from marine biomass, and type III, which originates from terrestrial biomass.

The relationship between biomass, biochars, coals, and kerogens can be presented as atomic ratios of key organic elements H/C vs. O/C with a Van Krevelen diagram, shown schematically in Figure 1. Dirk Van Krevelen originally developed these diagrams to assess and compare the compositions of coal samples.[6,7] Biomass, a collective term used to describe a wide range of plant-derived materials, occupies a large area at the top right corner of the diagram in Figure 1, indicating the presence of relatively large amounts of oxygen and hydrogen in its structure. On the other hand, the three materials derived from biomass—biochars, coals, and kerogens—occupy more discrete bands, indicating their distinct properties and chemical compositions.[4]

Please cite this article in press as: Wood et al., Developing a molecular-level understanding of biochar materials using public characterization data, Cell Reports Physical Science (2024), https://doi.org/10.1016/j.xcrp.2024.102036

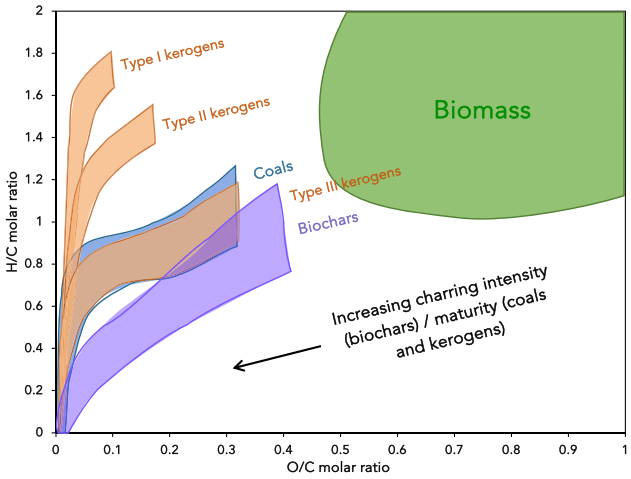

Figure 1. A schematic guide to the relationship between carbonaceous materials (biomass, biochars, coals, and kerogens)

Shown as a Van Krevelen diagram; data are taken from Surup et al.,[8,9] Smidt et al.,[10] Bakshi et al.,[11] Domingues et al.,[12] Pereira et al.,[13] Brewer and Brown,[14] Tintner et al.,[15] and Suliman et al.[16]

Biochars, coals, and kerogens originate from biomass and begin their existence with chemical compositions not vastly dissimilar from it. However, with increasing processing (for biochars) or maturity (for coals and kerogens), hydrogen and oxygen are lost from these materials, leading to a relative increase in carbon content and a decrease in H/C and O/C ratios.

While the chemical compositions of coals and type III kerogens almost entirely overlap—a consequence of their similar origins (lignocellulosic biomass)—the compositions of biochars are distinct. This divergence is evidence of the differences between the structures created during pyrolysis (higher temperature, shorter times) and the natural maturation (higher pressure and geological timescale) of biomass.[4,17] Nevertheless, biochars possess enough similarity to coals and kerogens to allow the analytical techniques used in characterizing those materials to be transferred into their study.

Feedstocks and plant biomass

Any form of dried biomass can be used to produce a biochar. Plant biomass, commonly derived from agricultural waste, such as sawdust, wood chips, straw, or husks, is a notable example. It can be thought of as consisting of two fractions—an organic fraction, containing carbon-rich molecular structures, and an inorganic fraction, containing a range of mineral compounds and water. An example schematic composition of dried plant biomass is shown in Figure 2.

The organic fraction of plant biomass consists primarily of three types of biopolymers: cellulose, hemicellulose, and lignin. Upon pyrolysis, these biopolymers thermally decompose in characteristic manners to produce biochar, bio-oil, and syngas.

Figure 2. Biomass composition

A schematic representation of a macromolecular composition of plant biomass after drying.

Please cite this article in press as: Wood et al., Developing a molecular-level understanding of biochar materials using public characterization data, Cell Reports Physical Science (2024), https://doi.org/10.1016/j.xcrp.2024.102036

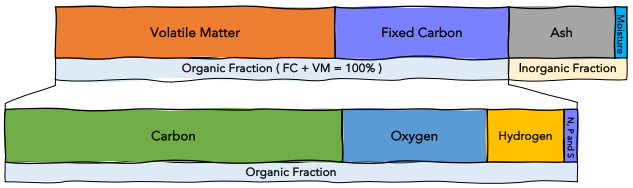

Figure 3. A schematic guide to the chemical composition of biochars

The upper band depicts the composition of a material, including both organic—volatile matter (VM) and fixed carbon (FC)—and inorganic—ash and moisture—fractions; the lower band depicts the elemental composition of the organic fraction only.

Cellulose and hemicellulose have low thermal stabilities and decompose between temperatures of approximately 300°C–400°C and 200°C–300°C, respectively.[18–20] During their decomposition, a large proportion of their mass are lost as bio-oils and syngas; thus, as a result, cellulose and hemicellulose contribute only moderately to biochar yields.[18,19,21] Lignin polymers have higher thermal stability, and their thermal decomposition occurs across a wide temperature range due to their heterogeneity, beginning at approximately 200°C and continuing to temperatures as high as 900°C.[18,19] Lignins decompose with relatively low mass loss and are, therefore, the main contributors to biochar yields.[18–22]

The relative quantities of cellulose, hemicellulose, and lignin within a feedstock heavily influence the properties of the biochar it produces.[19,21,23,24] Lignin polymers have the highest carbon content and are often considered the most influential of all biopolymers for biochar formation. Due to lignin's carbon content and stability, lignin-rich feedstocks are generally found to produce highly carbonized biochars.[25]

The mineral constituents of biomass are mostly non-volatile and are primarily converted to pyrolysis ash. As a result, feedstocks with high mineral content produce biochars with high ash contents, while those with low mineral content produce biochars with low ash contents.[12,13,26–28] These inorganic minerals are also known to have both catalytic effects, which can promote a variety of reactions during the carbonization process, and stabilizing effects, which may protect or inhibit the decomposition of certain molecular structures.[1,12,23,26,29–31] As a result, high-ash biochars may contain distinctly different molecular structures than their low ash counterparts.[12,32]

CHARACTERIZATION OF BIOCHARS

In the following section, we discuss the characterization of biochars, focusing on the different methods used and the molecular descriptors obtained. Owing to the variety of techniques available, many properties of biochars can be measured. However, it is essential to understand the limitations and sources of error within these measurements, as well as how different techniques can complement each other to obtain a holistic understanding of the properties of biochars.

Chemical composition

The chemical composition of a biochar can be determined through proximate and ultimate analyses. The proximate analysis allows for the identification of fractions of moisture, fixed carbon (FC), volatile matter (VM), and ash in a material. In contrast, the ultimate analysis provides insights into the discrete elements within the material. Figure 3 shows a schematic representation of biochar composition that can be obtained through these methods, respectively.

As with biomass, biochars can be thought of as being composed of organic and inorganic fractions, as shown in Figure 3.[14] The organic fraction consists of heterogeneous organic matter with varying thermal stabilities: components that are stable at high temperatures are known as FC, while those which decompose at high temperatures are known as VM.[5,33] At room temperature, however, both FC and VM exist as solids. The inorganic fraction of a biochar consists of ash and a small amount of residual moisture.

Proximate analysis has its roots in coal chemistry, where it is used to determine the fractions of moisture, ash, VM, and FC in a material at an operational temperature of 950°C.[5] It has been translated into the study of biochars and is now one of the most commonly used characterization techniques within biochar research.[16,23,26,29,34–36]

Traditionally, proximate analyses are carried out using the standard procedures detailed in ASTM D1762-84, "Standard Test Method for Chemical Analysis of Wood Charcoal."[33] In brief, moisture is defined as the mass lost when a sample is heated to 105°C in an inert atmosphere, VM is defined as the mass lost (minus that due to moisture) when a sample is heated to 950°C in an inert atmosphere, and ash is the mass remaining after combustion of a sample at 750°C. FC is then calculated by difference. Uncertainties in these measured values primarily arise from unwanted or unaccounted-for mass changes during heating/combustion (e.g., adsorbed atmospheric moisture, partial combustion, volatilization of ash compounds), fluctuations in the temperature of the furnace, and sample inhomogeneity.[5,36,37] Averaging across multiple measurements helps to reduce the error.

More modern techniques, based upon thermogravimetric analysis (TGA), are also used and measure mass loss *in situ* throughout the heating process.[16,27,36,38,39] TGA-based proximate analyses can be automated through use of a preset heating program, making it more convenient and reliable than the traditional method. However, TGA is still susceptible to many of the same issues outlined above, and, since very small sample sizes are often used, TGA-based analyses can be especially affected by sample inhomogeneity.[36] Averaging across multiple samples is, therefore, essential when using TGA.

Although useful for determining the proportions of inorganic to organic matter within biochars, proximate analyses provide no absolute insights into their molecular structures. These molecular structures must, therefore, be characterized using other techniques. Nevertheless, knowing the ash and moisture content of a sample is critical when carrying out further characterization as, often, both ash and moisture can strongly interfere with results.[23,26,36,40] In many cases, samples may be dried and de-ashed before any further characterization to limit these effects, particularly for high-ash biochars.

The organic fraction of a biochar consists predominantly of carbon, hydrogen, oxygen, and, to lesser extents, nitrogen, phosphorus, and sulfur (Figure 3). The relative amounts of these elements within a biochar sample are measured by ultimate analysis.

Ultimate analyses rely on the characterization of the gases produced after the complete combustion of a dried sample of known mass in an oxygen-rich atmosphere. The gases produced are collected and separated, and the quantities of CO_2, H_2O, N_2, and SO_2 are determined. These are then used to calculate the organic C, N, H, and S contents, respectively, of the original sample. While the O content can,

in principle, be determined by CNHS analyzer, in practice, this is often done based on the assumption that the quantities of other elements in the sample are negligible, so the amount of oxygen is calculated as a difference.[36]

To gain insights into the molecular structures within biochars, the elemental composition determined by ultimate analysis must only correspond to the organic fraction of a sample. However, biochar ash often contains carbon in the form of carbonates,[41] resulting in a measured C content corresponding to both the total organic and total inorganic carbon (TOC and TIC, respectively) fractions.[36,37] To remove the influence of these carbonates, samples should be washed before analysis, yet in many cases, this is not carried out.[9,11,12,29,42–47] When the ash content of a sample is low, this is passable, as the contribution of the TIC to the total carbon (TC) content is likely negligible, and so the TOC can be approximated as the TC.[11,26] However, when the ash content of a sample is high, the TC is not a good indicator of the TOC and should not be used as such.[26] Knowledge of a sample's ash content via proximate analysis is, therefore, required when examining the results of an ultimate analysis. Furthermore, in highly carbonized biochars with significant amounts of combustion-resistant carbon, incomplete combustion can also be problematic and lead to an underestimation of C contents. Utilizing a combustion catalyst can help reduce this occurance.[36]

Within biochar research, the results of ultimate analyses are often used to calculate molar H/C and O/C ratios.[11,12,15,16,22,48–52] These ratios can be used to assess the extent of carbonization of a sample—with lower H/C and O/C ratios indicating a higher degree of carbonization—and are often presented against each other in a Van Krevelen diagram, such as that shown in Figure 1.[8–16] Strictly speaking, these ratios should be calculated using only the TOC content to give clear insights into the carbonization of the organic matter within biochars.[5] However, in cases where the organic C content has not been explicitly measured, these ratios are usually calculated using the TC contents.[9,12,43–46] As a result, many of the reported H/C and O/C ratios of high-ash biochars may be misleading.[11]

Ultimate analyses provide direct insights into the elemental compositions of biochars and are, therefore, useful when attempting to represent their molecular structures. However, due to the multitude of ways in which atoms can be arranged while retaining the same elemental composition,[53] ultimate analyses alone cannot be used to predict the molecular structures within a sample.

Aromatic molecular structures

The aromatic molecular structures within biochars can be defined by their aromaticity indices (the proportion of aromatic carbons) and their aromatic domain sizes (the number of conjugated aromatic rings within polyaromatic domains).[34,50,54–60] The schematic in Figure 4 shows the relationship between these two properties. Three simple compounds that can be used as illustrative examples of these properties are benzene, naphthalene, and butylbenzene. Both benzene and naphthalene have aromaticity indices of 100%, whereas butylbenzene, with its alkyl group, has an aromaticity index of 60% (6 out of 10 carbons being involved in aromatic molecular structures). Both benzene and butylbenzene have aromatic domain sizes of one ring, whereas naphthalene has an aromatic domain size of two rings. This exemplifies the importance of both properties when attempting to define the aromatic molecular structures within a biochar.

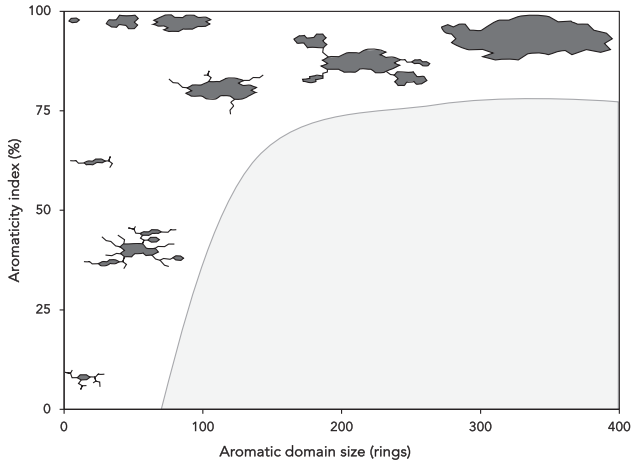

Figure 4. Aromaticity in biochars

Schematic guide to the aromaticity indices and aromatic domain sizes of biochars.

^{13}C solid-state nuclear magnetic resonance (ssNMR) can detect the various chemical environments within a biochar sample. It is then possible to calculate its aromaticity index using the relative proportion of aromatic and non-aromatic chemical environments.[34,56,59,60] Highly conjugated aromatic chemical environments can, however, be challenging to observe/detect using a typical ^{13}C ssNMR setup[34,58,60,61] and can lead to errors when calculating aromaticity indices of highly carbonized biochars. Alternative setups can be used to reduce this effect,[58,60] yet complex spectra and difficulties in deconvoluting peaks may still yield relatively high uncertainties when calculating aromaticity indices.

Aromatic domain sizes are even more difficult to characterize, though a number of techniques have been developed.[34,50,52,56–63] The simplest method uses H/C to estimate the average aromatic domain size, *n*, of a biochar.[52,59] This is performed by solving Equation 1 for *n*, following the assumption that all organic carbon within the sample is in the form of 6-membered aromatic rings solely consisting of C and H and that aromatic domains are distributed as a 2-dimensional grid of $\sqrt{n}$ by $\sqrt{n}$ aromatic rings, as shown in Figure 5A.[52] Aromaticity indices are then assumed to be 100%.

$$\frac{H}{C} = \frac{2\sqrt{n}+1}{n+2\sqrt{n}} \qquad \text{(Equation 1)}$$

Generally, the aromatic domain sizes predicted using this method are expected to be underestimated when the actual H/C is higher than the idealized one (from the Equation 1) for the same domain size. The H/C ratio will be higher when aromatic domains are distributed irregularly, yielding a more significant number of aromatic edge sites (as shown in Figure 5B) and/or when functional groups with higher H/C than defined in the Equation 1 are present (as shown in Figures 5C and 5D). Only in a small number of cases will the functional groups or carbon atom substitutions reduce the overall H/C ratio (as shown in Figure 5E), and then the aromatic domain sizes will be overestimated. Despite these apparent downfalls, this method offers a quick and easy route to estimating aromatic domain sizes within a sample. However, these values should generally be taken only as rough guides.

High-resolution mass spectrometry (MS) is a collection of techniques, all based upon the separation of ionized particles by their time of flight in the electromagnetic field.

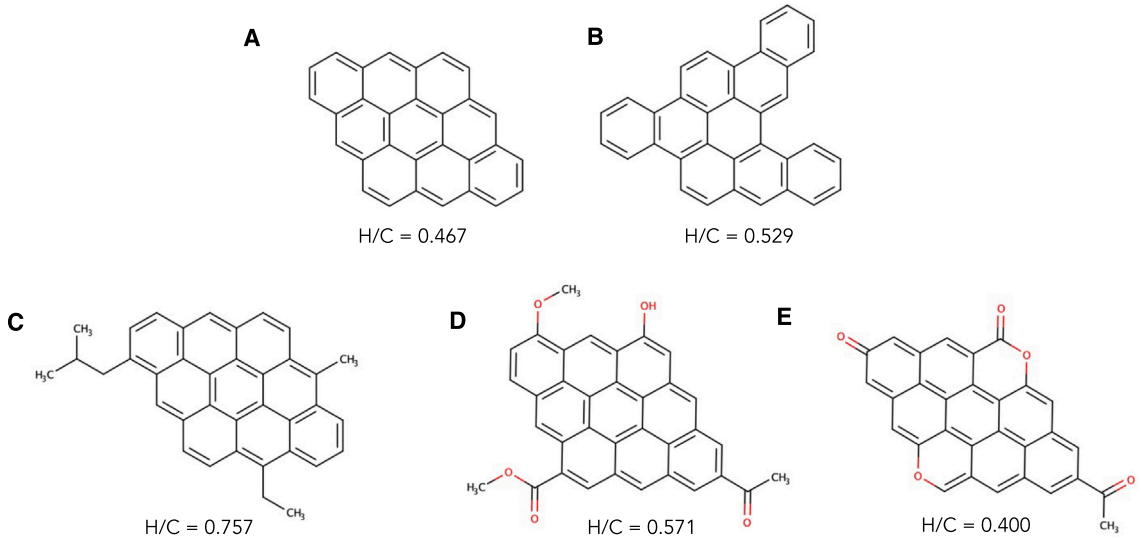

Figure 5. Characterization of aromatic domain sizes
Variation in H/C ratio for structures with the domain size of nine rings.

The MS instrument measures the mass-to-charge ratio that can be matched to the known molecular fragments; for example, spacings of 14 Da indicate N+, as well as CO2+ and CH2+, and spacings of 72 Da indicate C_6 (i.e., aromatic moieties).[29,64–66] Furthermore, the separation provide insights into the shape and interaction of the domains with the electromagnetic field. There are many types of MS, depending on the methods of ionization and detection. There are two major techniques of ionization—electrospray ionization, which first requires the sample to be in a solution, and laser-desorption ionization (e.g., MALDI), which applies rapid heat to vaporize the sample. Therefore, when it comes to the solid amorphous material, such as biochar, the main limitation of MS is in the accessibility of the structures for ionization, i.e., the obtained results are unlikely to be representative of the overall material.[23,47,66–68] However, the information obtained will still yield interesting and useful insights into the molecular structures within a biochar sample and, especially, their aromatic domain sizes.

Aromaticity indices and aromatic domain size distributions must both be known to capture the aromatic molecular structures within biochars. However, more information is still needed to describe these molecular structures' morphologies and how they pack together into nanostructures within the overall material.

Graphitization and crystallinity

Carbon-rich materials can be thought of as either graphitizing or non-graphitizing, as shown in Figure 6.[54,69] Graphitizing materials are those that form nanostructures resembling crystalline graphite when treated at temperatures of 2,200°C–3,000°C, while non-graphitizing materials are those that resist this ordering process and remain largely amorphous even when heated to temperatures exceeding 3,000°C.[54,70] The structural differences between these two types of materials are believed to result from the formation of defects, such as non-hexagonal rings, within their aromatic nanostructures.[66,70–80] These defects introduce curvature and act to disrupt packing and limit long-range ordering. In general, biochars possess only minimal graphitic crystallinity and, though rarely heated to temperatures as high as 2,200°C, are thought to be non-graphitizing.[8,9,55,81–84]

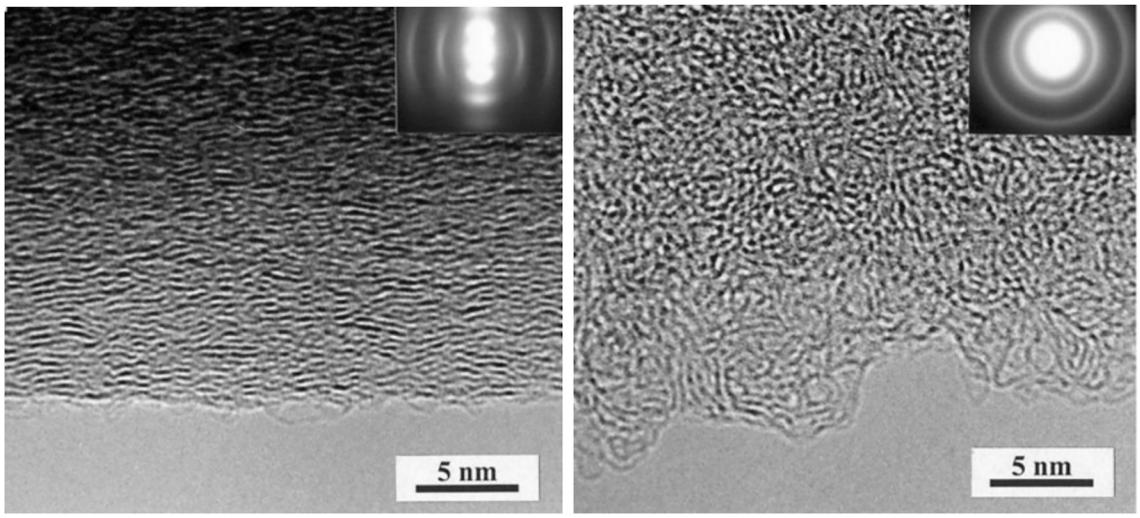

Figure 6. HRTEM images of carbon prepared from graphitizing anthracene and non-graphitizing sucrose at 1,000°C
Graphitizing anthracene shown at left and non-graphitizing sucrose shown at right. Insets show the diffraction pattern of the area. Reprinted from Harris et al.[72] Copyright 2000, with permission from Taylor & Francis.

The morphologies and nanostructures within biochars can be challenging to define in absolute terms. As a result, many techniques used to characterize these nanostructures yield only qualitative or relative results. These are, nevertheless, incredibly useful when attempting to understand biochars on the molecular level.

High-resolution transmission electron microscopy (HRTEM) can be used to image nanoscale regions of a biochar sample and can produce micrographs with up to atomic-level resolutions. From these, a wide range of features can be identified, including pentagonal, hexagonal, and heptagonal rings, graphitic and non-graphitic regions, and a range of different nanostructures.[8,9,47,55,82,84–86] However, due to the extremely high magnifications used, sample inhomogeneity can heavily bias the results of an HRTEM analysis. To reduce this, many areas of the sample should be imaged to obtain a representative overview of the sample and its nanostructures.

It is also possible to use HRTEM to visualize individual components of a biochar by first carrying out solvent extraction and liquid-phase exfoliation.[47,64,68] While this provides exciting and specific insights into the molecular structures, the methods through which individual components are removed are biased toward those that can be displaced from the main sample. As with MS, these components may not be representative of the overall material, and analysis of these alone may yield a biased view.

Raman spectroscopy is often used in conjunction with TEM[8,9,55,84,85] to detect Raman-active vibrational modes (those which scatter radiation inelastically) within a sample. Within Raman spectra, the presence of a peak centered around 1,590 cm^{-1} can be attributed to ordered graphitic nanostructures, such as those of crystalline graphite, and the presence of a broad peak centered around 1,350 cm^{-1} can be attributed to defective or disordered nanostructures, such as those present in non-graphitizing materials.[55,84,85,87] These two peaks are referred to as G and D peaks, respectively. Simply, the presence of a D peak in the Raman spectrum of a biochar indicates disorder within its nanostructures, yet the relative extent of disorder in a sample can also be assessed through comparison of the D

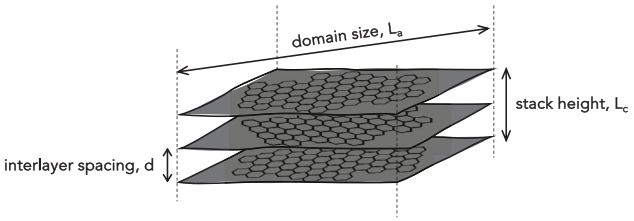

Figure 7. Diffraction analysis
A schematic guide to the interlayer spacing, domain sizes, and stack heights of graphitic crystallites within biochars.

and G peak areas[9,88–91] or peak intensities.[30,64,84,85,89,92,93] A low D-to-G ratio indicates a relatively low degree of disorder, whereas a high D-to-G ratio indicates a relatively high degree of disorder.[55,74,77,89,91] This D-to-G ratio gives relative information about the nanostructures within a biochar and can be used to compare between samples but not to obtain absolute measures. However, as both peak areas and peak intensities, along with a range of different deconvolution procedures, are used throughout the literature, many D-to-G ratios are not directly comparable.[69,84,87,89–91,94,95] Furthermore, excessive grinding of a sample, which may mechanically introduce defects and add to the D peak,[88,95] or unintentional heating of the sample by the incident radiation, which may lead to peak shifting, can also be sources of error and uncertainty when characterizing biochars using Raman spectroscopy.[91]

Despite biochar's very limited graphitization, short-range graphitic structures have been found within them.[9,23,47,55,84,96] These graphitic nanostructures are thought to consist of nanoscale regions of π-π stacked aromatic sheets, often referred to as crystallites.[54] When analyzed by X-ray diffraction or electron diffraction (ED), crystallite-containing biochars produce diffractograms characteristic of crystalline graphite.[10,23,45,46,55,81,96–98] The inserts of Figure 6 are the selected-area ED patterns carried out alongside TEM. These patterns demonstrate the symmetric diffraction rings of amorphous structure and arcs, confirming layer alignments for the graphitizing structure, with the short sharp peaks corresponding to the {002} interlayer spacings. The diffraction pattern is an overlay of signals, which can be deconvoluted through Fourier transform (FT) and then used to calculate the interlayer spacing, average domain size, and stack height of crystallites within the sample (Figure 7).

The Bragg's law defines a geometric relation between atomic planes and the scattering angles at a given wavelength,[99,100] and so it allows the interlayer spacings within the crystalline material to be calculated. Knowing the X-ray's wavelength allows for determining the atomic distances, producing sharp peaks for an orderly crystal. Nevertheless, stacking faults and disordered materials will result in broader, overlapping peaks with lower intensity, creating the uncertainties in the measured distances.

On the other hand, the average domain sizes and stack heights of crystallites are calculated using the Scherrer equation, which is based on the idea that crystallites of <200 nm cause peak broadening in a diffractogram.[101] However, there is some debate as to whether this holds true in complex carbonaceous materials, as the Scherrer equation does not account for the many other factors that can also contribute to this peak broadening,[102] for example, instrumental effects, curvature caused by strain within the crystallites, and defects, such as dislocations and grain

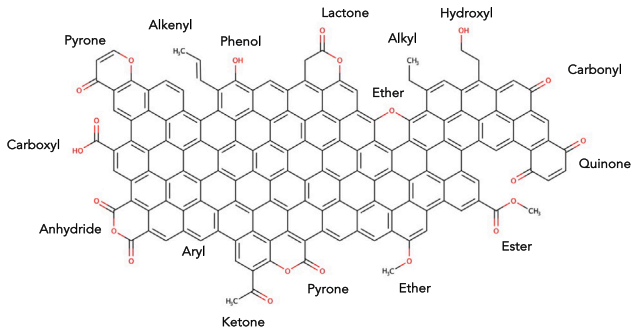

Figure 8. Functional groups diversity
Examples of types of carbon- and oxygen-based functionalities present within biochars.

boundaries, within the nanostructures of a sample.[102] In biochars, it is near impossible to determine which of these many factors is the main source of peak broadening. Furthermore, the Scherrer equation uses a shape constant, *K*, to calculate the average domain sizes and stack heights within a biochar sample.[101] This constant must be chosen to represent the shapes of fragments within crystallites, yet, for biochars, this shape is unknown. Many different values of *K* have been suggested, but a consensus has yet to be reached.[37,45,103–106] As a result, the calculated average domain sizes and stack heights will vary depending on the chosen *K* value. Other causes of uncertainty in these calculated values may arise due to peak asymmetry, noise/background scattering, and/or issues when fitting curves to peaks.[37]

These techniques give complementary insights into the aromatic molecular structures within biochars and can be combined to gain an overview of the nanostructures present within a sample.

Functional groups

Biochars contain significantly fewer functional groups than their biomass precursors. These are related, through chemical transformations, to those found within biomass. Carbon- and oxygen-based functionalities dominate, including aryl, hydroxyl, carbonyl, and many more. Examples of these are shown in Figure 8.[49,92,96,107–118] Depending upon the composition of the starting biomass, a variety of nitrogen-, phosphorous-, and sulfur-based functionalities may also be present; nevertheless, those are found in significantly lower quantities than oxygen-based groups.[116,119]

Depending on its origin, the biomass may contain a wide variety of functional groups; nevertheless, many become unstable during pyrolysis. As a result, the range of functional groups present within biochars is much more limited. The approximate stabilities of a variety of common oxygen-based functional groups are shown in Figure 9. From this, we can see that each functional group decomposes across a wide temperature range, as opposed to at a single value. This is due to the influence of the chemical environment surrounding a group. This effect is particularly of note in the production of biochars, as a range of factors will affect how functional groups develop during pyrolysis. For example, as previously mentioned, inorganic compounds can have both catalytic and stabilizing effects, and so the presence of these compounds may significantly affect the decomposition and/or transformations of functional groups when producing a biochar.[12] Feedstock inhomogeneity may exacerbate this effect and result in significant variation in the functional groups of the produced biochar.[120] Nevertheless, from Figure 9, we can see that certain functional groups (e.g., carbonyls and pyrones) are more stable than others (e.g., carboxyl). At

Please cite this article in press as: Wood et al., Developing a molecular-level understanding of biochar materials using public characterization data, Cell Reports Physical Science (2024), https://doi.org/10.1016/j.xcrp.2024.102036

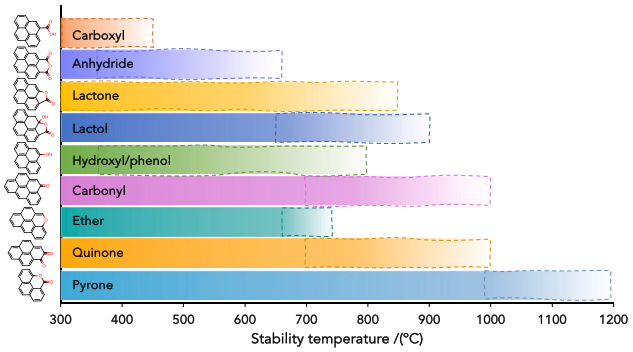

Figure 9. A schematic guide to the stability of oxygen-containing functional groups

Colored bars indicate temperatures at which each functional group is stable, and dashed areas indicate approximate temperature ranges at which each functional group becomes unstable. Data are from Li et al.,[121] de la Puente et al.,[122] Otake and Jenkins,[123] Zhuang et al.,[124] Zielke et al.,[125] Marchon et al.,[126] Figueiredo et al.,[127] Samant et al.,[128] and Figueiredo and Pereira.[129]

the same time, the carboxylic group in a highly acidic form will decompose 100° earlier than its weakly acidic counterpart where H-bonding with neighboring atoms will stabilize it.[121]

Despite only being present in relatively low numbers, the functional groups within biochars are central to how biochars interact with their surrounding environment. A holistic understanding of these functionalities, particularly those exposed on surfaces, is, therefore, crucial when building a molecular-level understanding of these materials. A combination of analytical techniques can be used to achieve this.

FT infrared (FTIR) spectroscopy is most commonly used to characterize the functional groups within biochars by probing their vibrational frequencies.[92,96,110–114] This is typically done by detecting IR frequencies reflected by the surface of a sample.[25,36,37,130–132] However, low resolutions and difficulties in assigning peaks, particularly when broad or overlapping peaks are present, can be problematic when attempting to characterize the functional groups using FTIR. These spectral features make it difficult to confidently distinguish between functionalities, and so only a loose identification of functional group is often possible.

X-ray photoelectron spectroscopy (XPS) also offers insights into the functional groups present within biochars by probing atomic environments upon the surface of a sample, typically up to ~10 nm depth.[16,36,115–117] The relative quantities of sp^2 and sp^3 carbons, aromatic carbons, and single and double-bonded oxygens within a sample can be identified in this way. As a highly sensitive surface technique, XPS is strongly influenced by contamination, oxidation, or the presence of moisture upon the surface being examined, and so samples should be prepared *in situ* to yield accurate results.[36]

The acidic functional groups within biochars can be distinguished through their dissociation constants (pK_as). Strongly acidic groups, such as carboxylic acids and anhydrides, can be neutralized with weak bases, while mildly acidic groups, such as lactones, and weakly acidic groups, such as hydroxyls and phenols, require progressively stronger bases.[36,107–109]

Boehm titrations utilize these differences in acidity to determine the amounts of strongly acidic, mildly acidic, and weakly acidic functional groups present upon

the surface of a sample, which, in biochars, are assumed to be carboxyl, lactonic, and phenolic functional groups, respectively.[16,36,39,49,118,133] The method is, in principle, straightforward—the carbon material is first treated with a reaction base, which is neutralized by the most acidic functional groups, and second, the remaining base is quantified by the acid-base titration. The standard bases from pK_a = 6.4 ($NaHCO_3$) to pK_a = 20.6 (NaOEt) are used and are assumed to neutralize all oxygens that are more acidic.[108] These titrations were originally developed to analyze carbonaceous materials with negligible ash content[107–109] and so will be affected by the presence of ash within a sample due to the pH-altering effects of soluble inorganic species.[36] Ash and any other buffering materials should, therefore, be removed prior to analysis, yet this is infrequently carried out and may lead to incorrect results.[16,39,49,118,133]

When characterizing biochars, FTIR, XPS, and Boehm titrations will only detect functional groups that are either exposed (or very close) to the samples surface. The extent of sample grinding prior to analysis likely influences results. Although finely ground samples offer the most complete overview of the functionalities present within the overall biochar, the grinding process may mechanically alter the molecular structures within a sample and lead to skewed results.[88,95,134–137] On the other hand, the analysis of unground samples may yield unrepresentative results and can be heavily influenced by sample inhomogeneity. A combination of the above techniques should be used to gain complementary insights into the functionalities present within a biochar sample.

pH_{pzc} and pH

Adding a biochar to a solution will cause a change in pH due to the presence of minerals, soluble inorganic species, and the protonation/deprotonation of acidic/basic functional groups at the surface. In solution, these groups will protonate and deprotonate in accordance with their pK_as, allowing the biochar surface to become positively or negatively charged.

Two pH-related properties are often measured in biochar research: the "pH" of the biochar, which gives an indication of the overall acidity or basicity of a sample and is measured as the pH at which a solution containing biochar equilibrates, and the point of net zero charge (pH_{pzc}), which is a measure of the pH at which the net surface charge of biochar is zero and is calculated as the pH at which the addition of biochar to solution results in no change in pH.[12,26,27,36,42,49,110] However, both measures are dictated by ash and soluble inorganic species and give relatively limited insight into the functional groups present within the organic fraction of a biochar.[12,16,26,49,138] Furthermore, both pH and pH_{pzc} are heavily dependent on experimental setup, and the lack of standardized protocols renders many literature values incomparable.

Density and porosity

Biochars are mesoporous materials with pore size distributions (PSDs) spanning multiple length scales. These pores are divided into three categories based on their diameters: macropores with diameters between 0.05 and 1,000 μm, mesopores with diameters between 2 and 50 nm, and micropores with diameters less than 2 nm.[1] Generally, the macropores within a biochar sample are determined by the structures of the feedstock.[16,36,97,139] Meso- and microporosity develop throughout the pyrolysis process as volatiles escape the solid matrix.

The density of porous materials can be defined in several ways depending upon the extent to which pores are included in the volume measurement. Three density

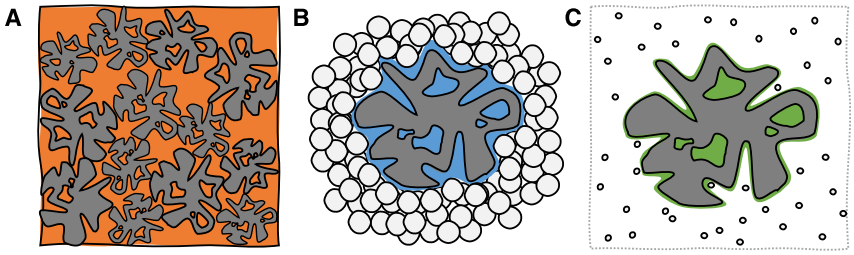

Figure 10. Schematic guide to the densities of biochars

Biochars shown in gray. (A) shows the volume measured (in orange) when calculating bulk density, (B) shows the volume measured (in blue) when calculating envelope density, and (C) shows the volume measured (in green) when calculating true density.

measures are relevant to the study of biochars: bulk density, envelope density, and true density. These densities and their corresponding volumes are depicted in Figure 10.

Bulk density, also known as packing density or tap density, is the simplest measure of density. It is found by adding a known sample mass to a container and measuring its volume after vibrating or tapping to obtain optimal packing of particles. Bulk densities include the volumes of the particles themselves, the pores within them (intra-particle pores), and the voids between them (extra-particle voids) (Figure 10A). Therefore, they largely depend on the sizes and shapes of particles within a sample—with those that can pack together more effectively returning higher bulk densities.

Envelope density, also known as apparent density or particle density, is a more refined measure of density. It represents the average density of individual particles within a sample, including intra-particle pores, while excluding extra-particle voids. The envelope density of a sample can be calculated by measuring the volume displaced when a known mass of the sample is completely immersed and consolidated in a container of smaller non-wetting particles.[36,44] In this way, the volumes of only the biochar particles and their intra-particle pores are included in the calculation of envelope density (Figure 10B). When carrying out this measurement, it is important that the non-wetting particles completely surround and pack tightly around the sample. The sizes of non-wetting particles, the forces used to consolidate them, and the ratio of sample to non-wetting particles can therefore significantly impact results.[44] The non-wetting particles should be small enough, the consolidation force should be high enough, and the ratio of sample to non-wetting particles should be low enough to ensure that all extra-particle voids are occupied. However, consolidation forces that are too large may cause the fracturing of particles and should, therefore, not be excessively high.[44]

True density, also known as skeletal density or helium density, is the finest measure of density. It represents the average density of individual particles within a dried sample, excluding intra-particle pores and extra-particle voids. True densities are measured using helium pycnometry. This technique uses the isothermal expansion of helium gas to calculate the volume occupied by a sample. It is assumed that helium gas can penetrate all open/accessible intra-particle pores and, therefore, that only the volumes of the particles themselves and any closed/inaccessible intra-particle pores are included in the calculation of true density (Figure 10C). This is an important assumption when calculating true densities, as changes to particle sizes (e.g., through grinding) can expose additional intra-particle pores and thereby

increase the measured true density of the sample.[44] Fine grinding prior to analysis can reduce this variability by exposing the maximum number of intra-particle pores, thus allowing comparison between samples.[44] Degassing to remove adsorbed moisture, volatile compounds, and/or tarry substances, which can also block pores and lead to error, is also recommended.[36] Furthermore, as the closest approach of a helium atom to the surface of a sample is its collision radius (~1.3 Å),[140] a volume near the surface will be excluded from analysis.[140] In materials with very high specific surface areas (SSAs), such as activated carbons that have SSA on the order of thousands of m^2g^{-1}, this excluded-volume effect can cause significant errors in results.[140–142] However, it has been shown to be negligible in biochar-like materials that have SSAs only on the order of hundreds of m^2g^{-1}.[140,142] A second important assumption made when calculating true densities by helium pycnometry is that helium does not adsorb to the samples surface. This, however, is not the case for all carbonaceous solids.[141,143,144] Adsorption effects become especially significant in high SSA materials,[140,141,144] and so, as with excluded-volume effects, adsorption effects have been shown to be negligible in biochars.[144] Further sources of error or uncertainty in these measured true densities can arise from insufficient equilibration or measurement cycles and sample inhomogeneity.[145] Generally, using 20+ equilibration cycles and averaging across 10+ measurement cycles are therefore recommended.[15,34,36,37,145]

True densities are of the most relevance when attempting to understand biochars on the molecular level, as they include only minimal porosity and therefore give the best indication of the density and packing of nanostructures within a sample. Comparison of the true densities of biochars to that of graphite can yield insights into the degree of aromatic condensation and graphitization of biochar: ash-free biochars have densities below that of graphite, indicating that they have lower degrees of aromatic condensation and less ordered nanostructures. The measured true density of a biochar, however, is an average of all different components within it, including both organic and inorganic fractions. This should be considered when using true densities of biochars to obtain information about their nanostructures. In general, the inorganic fraction of a biochar will have a higher density than the organic fraction,[34] and so, in high-ash biochars, the measured true densities will be slightly inflated.

When combined, envelope densities and true densities can also be used to gain insights into the porosity of a biochar as a percentage volume.[44,146] This porosity is calculated as the percentage difference between the densities measured by each technique and therefore represents the percentage volume of intra-particle pores within a biochar sample. However, this calculation is only valid when both measurements are carried out on samples with approximately equivalent particle sizes.[36]

A second technique used to characterize the densities and porosities of biochars is mercury porosimetry. Mercury is a non-wetting fluid and so will only enter the pores of a material under pressure. During a mercury porosimetry measurement, a sample is enveloped by mercury, and the pressure of the system is gradually increased, forcing the mercury to enter progressively smaller pores. The volume changes are measured throughout this process, allowing the porosity and PSD within a sample, along with its envelope and true density, to be calculated.[44] Mercury porosimetry can be problematic for biochars, as the high pressures may cause damage to the sample, leading to permanent changes in its pore structures and erroneous in results. Furthermore, although pores are assumed to be cylindrical when calculating PSDs, a range of different pore shapes/structures are likely to be present within biochars, and the diameter of pore openings may not be representative of internal pore

diameters. As a result, the calculated PSDs may differ from those within the sample. In addition, the contact angle between the mercury and the sample, which is used to calculate porosity and PSDs, is likely to vary greatly due to surface roughness and surface-exposed functional groups, yet this is infrequently considered.[9,44,147]

Surface area and porosity

Biochars have a relatively high SSA due to their porous nature. Gas adsorption is traditionally used to characterize these SSA, with N_2 and CO_2 being the most common choices of the adsorbate.[22,30,34,36,44,49,82,96,139,148–153] Gas adsorption techniques generally rely on applying adsorption models to calculate the SSAs of a sample of known mass from the relationship between the adsorbed amount and the adsorbate pressure. The choice of both adsorption model and adsorbate will affect these calculated properties.[37,149,151] Experimental setup can also significantly affect the adsorption isotherms of biochars. The degassing temperature, for example, has been shown to have strong effects due to the volatilization of organic and tarry compounds at increased temperatures.[151]

The Brunauer-Emmett-Teller (BET) model is most commonly used to calculate the SSA of biochars.[22,34,49,96,149,151,153] It assumes that all adsorption sites are equivalent, and so it is unsuitable for the characterization of heterogeneous or microporous materials.[148,154] Biochars, however, are both heterogeneous and microporous, which makes the BET model prone to incorrect result. Furthermore, the standard relative pressure range of 0.05–0.35 is often too large when applied to biochars and should be adjusted to ensure the validity of the BET model.[148,149,155,156] Although methods have been developed to aid in this adjustment,[148,155] the correct relative pressure range can be difficult to identify,[148,149] leading to further error and uncertainty.

The adsorption of N_2 at 77 K is typically used to determine the SSA of biochars. When using the BET model, the SSA of the sample is found by multiplying the molecular cross-sectional area of N_2 by the monolayer adsorbed amount and normalizing by the mass of the sample being analyzed. As a standard, the molecular cross-sectional area of N_2 is calculated assuming that molecules are adsorbed in a hexagonal close-packed monolayer.[148,154] However, N_2 has a quadrupole moment that can interact with polar surfaces, such as those of biochars, and lead to deviations from this standard value. As a result, BET SSAs of biochars calculated using the standard N_2 cross-sectional area may be significantly incorrect.[148,154] Hysteresis, long equilibration times, and micropore filling/condensation can lead to further errors. These issues may be overcome through the use of alternative adsorption models and/or alternative adsorbate gases.[148,154]

Gas adsorption can also be used to assess pore volumes and PSDs within biochars.[30,44,82,139,149–152] As with SSAs, this can be achieved through the application of adsorption models, such as the Barrett-Joyner-Halenda model,[30,98,132,139,148,157] or through computational techniques, such as density functional theory (DFT) and nonlocal DFT,[148–150,158] which use fluid dynamics to characterize pores.

The N_2 at 77 K is kinetically unable to access micropores <0.5 nm; instead, CO_2 at 273 K is often used when characterizing the pore volumes and PSDs of biochars.[148,149,156] The CO_2 isotherms can be analyzed in much the same way as N_2 isotherms; however, as CO_2 is only able to probe pores up to approximately 1.5 nm, only microporosities can be characterized using CO_2 adsorption isotherms.[148] Unfortunately, CO_2 possesses an even greater quadrupole moment than N_2 and so

Please cite this article in press as: Wood et al., Developing a molecular-level understanding of biochar materials using public characterization data, Cell Reports Physical Science (2024), https://doi.org/10.1016/j.xcrp.2024.102036

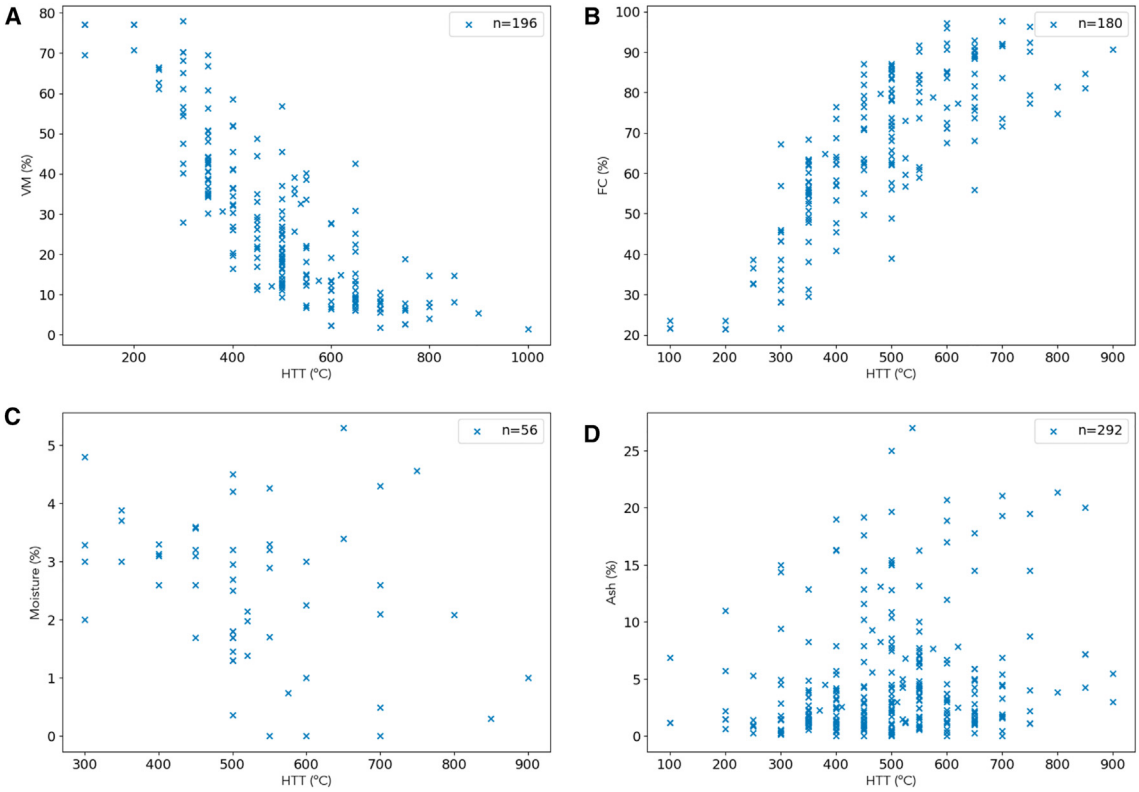

Figure 11. Influence of HTT on proximate composition of woody biochar

(A) VM, (B) FC, (C) moisture, and (D) ash as weight percent. The number of data points, *n*, for each plot is given in the legend.

may still yield unreliable results.[148,151,154,159] Gases such as Ar, O_2, and H_2, which have much smaller (or zero) quadrupole moments, have been proposed as alternatives and are likely, in the future, to replace N_2 and CO_2 in the characterization of biochars and biochar-like materials.[148,154,159–161]

HTT EFFECT ON BIOCHAR STRUCTURE AND PROPERTIES

Although many conditions can be varied during biochar production, the HTT reached during pyrolysis is widely accepted as the most influential of these.[27] As a result, thermo-sequences, in which biochars are produced across a series of HTTs, are often used when studying their properties. The temperature ranges studied generally range from as low as 200°C–300°C and reach highs of 1,000°C–1,200°C. Thus, the changes in biochar properties with increasing carbonization can be seen.

We collected data from the UKBRC Charchive (http://www.charchive.org), the UC Davis Biochar Database (http://biochar.ucdavis.edu/), and a number of published studies[2,15,38,44,48,56,58–60,146,162,163] in order to observe these effects, focusing solely upon biochars produced from woody feedstocks. The trends observed through these data are also true of other feedstock types.[2,12,16,25–27,58,164,165] The collected data can be downloaded from https://github.com/Erastova-group/Biochar_MolecularModels.

The influence of HTT on proximate composition is shown in Figure 11, and ultimate composition is shown in Figures 12 and 13. From these, we can clearly see that with increasing HTT, the FC content of biochars increases, while the VM content and H/C

Please cite this article in press as: Wood et al., Developing a molecular-level understanding of biochar materials using public characterization data, Cell Reports Physical Science (2024), https://doi.org/10.1016/j.xcrp.2024.102036

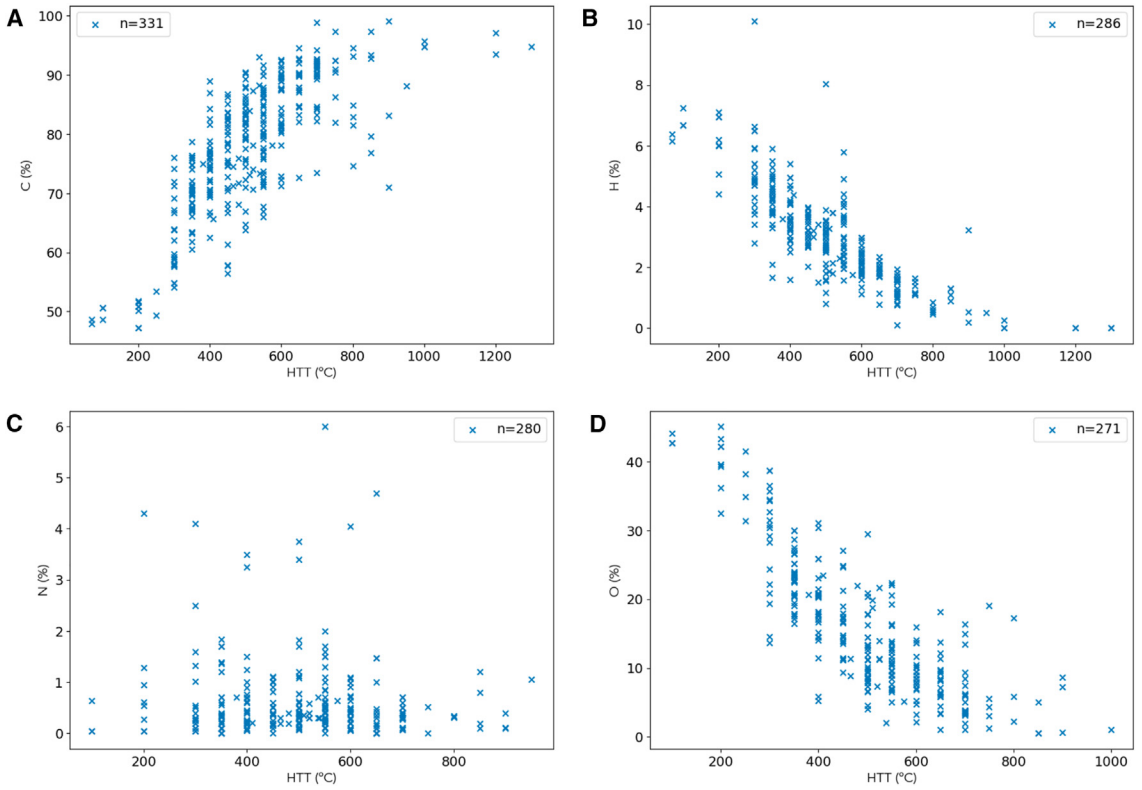

Figure 12. Influence of HTT on ultimate composition of woody biochar

(A) C, (B) H, (C) N, and (D) O contents as weight percent. The number of data points, *n*, for each plot is given in the legend.

and O/C molar ratios decrease. These changes correspond to the increase in carbonization of the organic matter within biochars with increasing HTT via the formation of stable carbon-rich molecular structures and the loss of oxygen- and hydrogen-rich volatile organic compounds. The effects of HTT on moisture and ash content (Figures 11C and 11D), however, are less obvious, as these components comprise much smaller fractions of the total biochar and are, therefore, more strongly influenced by the abovementioned characterization issues. In general, moisture slightly decreases with HTT, whereas ash becomes relatively enriched with an increasing HTT due to the loss of organic matter.

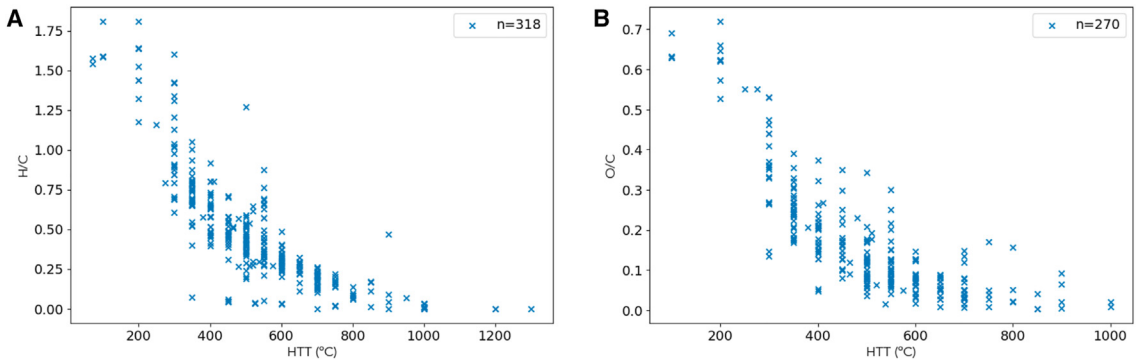

Figure 13. Influence of HTT on molar ratios

Effect on (A) H/C and (B) O/C molar ratios of woody biochars. The number of data points, *n*, for each plot is given in the legend.

Cell Reports
Physical Science
Perspective

CellPress
OPEN ACCESS

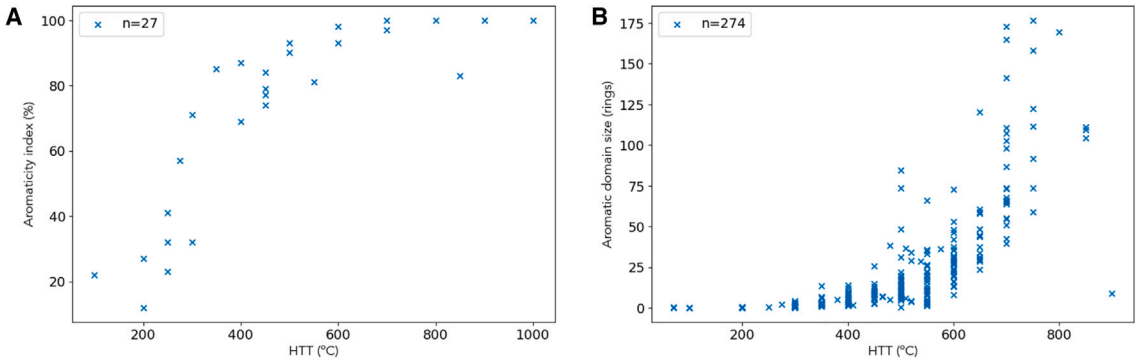

Figure 14. Influence of HTT on aromaticity

Effect on (A) aromaticity and (B) aromatic domain size of woody biochars. The number of data points, *n*, for each plot is given in the legend.

Figure 14 shows the influence of HTT on the aromaticity index and aromatic domain size. From this, we can see that both the aromaticity index and aromatic domain size increase with increasing HTT. While the aromaticity index increases fairly rapidly between 200°C and 500°C, aromatic domain size increases more gradually. This corresponds to the increase in carbonization of the organic matter within biochars with increasing HTT, first through the formation of smaller clusters of aromatic rings and then through the gradual condensation of these structures into a highly conjugated aromatic carbon network.

The influence of HTT on pH is shown in Figure 15. From this, we can see that pH generally increases with increasing HTT. While this change is primarily due to the increase in alkaline ash content (Figure 11D), it is also partly related to the loss of acidic functional groups (Figures 9 and 12B) from the organic matter of these biochars with increasing HTT.

The influence of HTT on the true density and SSA is shown in Figure 16. From this, we can see that the true density increases with increasing HTT and plateaus at a density of ~2,000 kg m^{-3}, just below that of graphite (density ~2,250 kg m^{-3}).[14,15,48] Again, this change primarily corresponds to the increase in carbonization of the organic matter of these biochars with increasing HTT. The surface area also appears to increase with increasing HTT; however, the larger

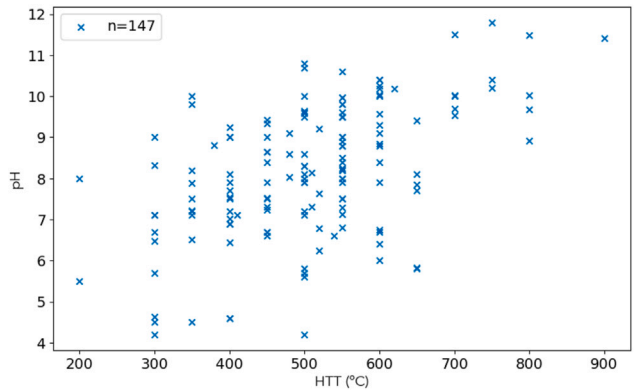

Figure 15. Influence of HTT on pH of woody biochars

The number of data points, *n*, for each plot is given in the legend.

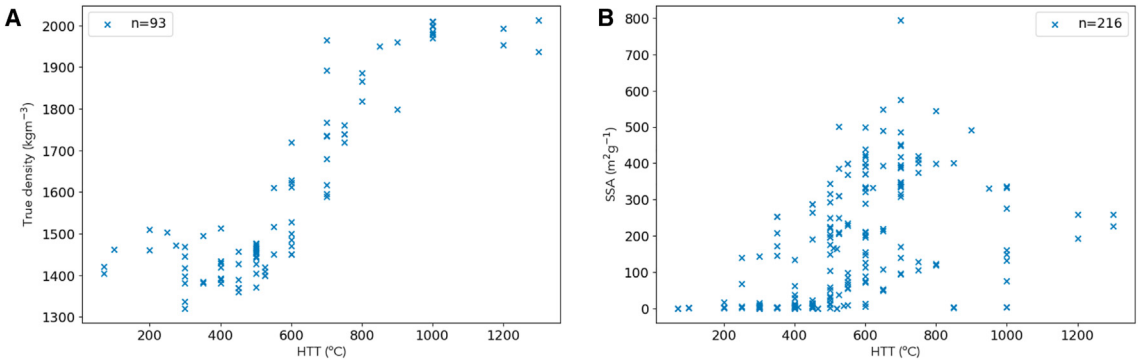

Figure 16. Influence of HTT on porosity

Effect on (A) true density and (B) specific surface area (SSA) of woody biochars. The number of data points, *n*, for each plot is given in the legend.

spread of data caused by the issues outlined earlier and the lack of data points at higher HTTs make this trend more challenging to discern. The increase in SSA with increasing HTT is due to the development of porosity, particularly micro- and mesoporosity, at increased HTTs. This porosity is formed as volatiles exit the biochar, leaving behind voids and channels and exposing additional surface.[164]

The influence of HTT on the functional groups within biochars is difficult to quantify numerically. However, these effects can still be observed and understood through a review of the literature. In woody biochars, functional groups will be predominantly oxygen based due to the woody feedstocks' low nitrogen, phosphorus, and sulfur contents.[12,26,96,116,119,164] Biochars produced at lower HTTs have lower aromaticity indices and, therefore, greater numbers and a wider variety of functional groups. With increasing HTT, both hydrogen and oxygen are lost (Figures 12 and 13), and, as a result, the total numbers of functional groups present will decrease. Furthermore, as many functional groups become unstable at high temperatures (Figure 9), the range of functional groups present will be reduced.[25] Biochars produced at high HTTs will be predominantly aromatic, with limited numbers of more thermally stable functional groups, many of which will be conjugated into the aromatic molecular structures of these materials.[25]

The aim of our work is to bring much-needed molecular-level understanding of biochar materials. Here, we present the first part of the work, where we have critically assessed the analytical techniques used to characterize biochars and, in doing so, assembled the information necessary to develop a molecular-level understanding of these materials. We have gathered and presented a large collection of characterization data, obtained from public domains, allowing us to gain insights into the changes in the chemical, physical, and molecular properties of woody biochars as a function of biochar's processing, quantified as the HTT. This information, supported by an understanding of limitations of each analytical technique, has allowed us to gain understanding of the molecular structures comprising woody biochars and thus paved the way for the next part of this work—the development of realistic biochar molecular models for simulations. Further analysis of the collected data and the development of a set of realistic biochar models for molecular simulations can be found in Wood et al.[3]

DATA AND CODE AVAILABILITY

All the data presented are openly available from https://github.com/Erastova-group/Biochar_MolecularModels, https://doi.org/10.5281/zenodo.10994175. The

data were derived from the following resources available in the public domains: https://www.charchive.org and https://biochar.ucdavis.edu.

ACKNOWLEDGMENTS

R.W. would like to thank the NERC Doctoral Training Partnership grant (NE/S007407/1) for the funding of her PhD project "Molecular Modeling for Design of Biochar Materials." V.E. thanks Chancellor's Fellowship by the University of Edinburgh.

AUTHOR CONTRIBUTIONS

R.W. has performed the literature review, collected and analyzed the data, and drafted the manuscript. All authors have contributed to the manuscript preparation and its review. All authors have jointly conceived the presented idea. V.E. supervised the project.

DECLARATION OF INTERESTS

The authors declare no competing interests

REFERENCES

1. Lehmann, J., Joseph, S., and Joseph, S. (2015). Biochar for Environmental Management (Taylor & Francis). https://doi.org/10.4324/9780203762264.
2. Weber, K., and Quicker, P. (2018). Properties of biochar. Fuel *217*, 240–261. https://doi.org/10.1016/j.fuel.2017.12.054.
3. Wood, R., Masek, O., and Erastova, V. (2023). Developing realistic molecular models of biochars. Cell Reports Physical Science *5*, 102037.
4. Burnham, A.K. (2017). Global Chemical Kinetics of Fossil Fuels: How to Model Maturation and Pyrolysis (Springer International Publishing). https://doi.org/10.1007/978-3-319-49634-4.
5. Speight, J.G. (2015). Handbook of Coal Analysis Second Edi (John Wiley & Sons, Inc). https://doi.org/10.1002/9781119037699.
6. Van Krevelen, D. (1950). Graphical statistical method for the study of structure and reaction processes of coal. Fuel *29*, 269–284.
7. Krevelen, D.W.V. (1993). Coal, Third Edition 3rd ed. (Elsevier).
8. Surup, G.R., Foppe, M., Schubert, D., Deike, R., Heidelmann, M., Timko, M.T., and Trubetskaya, A. (2019). The effect of feedstock origin and temperature on the structure and reactivity of char from pyrolysis at 1300–2800 °C. Fuel *235*, 306–316. https://doi.org/10.1016/j.fuel.2018.07.093.
9. Surup, G.R., Nielsen, H.K., Heidelmann, M., and Trubetskaya, A. (2019). Characterization and reactivity of charcoal from high temperature pyrolysis (800–1600 °C). Fuel *235*, 1544–1554. https://doi.org/10.1016/j.fuel.2018.08.092.
10. Smidt, E., Tintner, J., Nelle, O., Oliveira, R.R., Patzlaff, R., Novotny, E.H., and Klemm, S. (2020). Infrared spectroscopy refines chronological assessment, depositional environment and pyrolysis conditions of archeological charcoals. Sci. Rep. *10*, 12427–12511. https://doi.org/10.1038/s41598-020-69445-6.
11. Bakshi, S., Banik, C., and Laird, D.A. (2020). Estimating the organic oxygen content of biochar. Sci. Rep. 13082–13112. https://doi.org/10.1038/s41598-020-69798-y.
12. Domingues, R.R., Trugilho, P.F., Silva, C.A., Melo, I.C.N.A.d., Melo, L.C.A., Magriotis, Z.M., and Sánchez-Monedero, M.A. (2017). Properties of biochar derived from wood and high-nutrient biomasses with the aim of agronomic and environmental benefits. PLoS One *12*, e0176884. https://doi.org/10.1371/journal.pone.0176884.
13. Pereira, B.L.C., De, A., Carneiro, C.O., Márcia, A., Carvalho, M.L., Colodette, J.L., Oliveira, A.C., and Fontes, M.P.F. (2013). Wood Chemistry & Charcoal.
14. Brewer, C.E., and Brown, R.C. (2012). Biochar. In Comprehensive Renewable Energy (Elsevier), pp. 357–384. https://doi.org/10.1016/B978-0-08-087872-0.00524-2.
15. Tintner, J., Preimesberger, C., Pfeifer, C., Soldo, D., Ottner, F., Wriessnig, K., Rennhofer, H., Lichtenegger, H., Novotny, E.H., and Smidt, E. (2018). Impact of Pyrolysis Temperature on Charcoal Characteristics. Ind. Eng. Chem. Res. *57*, 15613–15619. https://doi.org/10.1021/acs.iecr.8b04094.
16. Suliman, W., Harsh, J.B., Abu-Lail, N.I., Fortuna, A.M., Dallmeyer, I., and Garcia-Perez, M. (2016). Influence of feedstock source and pyrolysis temperature on biochar bulk and surface properties. Biomass Bioenergy *84*, 37–48. https://doi.org/10.1016/j.biombioe.2015.11.010.
17. Kelemen, S.R., Afeworki, M., Gorbaty, M.L., and Cohen, A.D. (2002). Characterization of organically bound oxygen forms in lignites, peats, and pyrolyzed peats by X-ray photoelectron spectroscopy (XPS) and solid-state 13C NMR methods. Energy Fuels *16*, 1450–1462. https://doi.org/10.1021/ef020050k.
18. Zhao, C., Jiang, E., and Chen, A. (2017). Volatile production from pyrolysis of cellulose, hemicellulose and lignin. J. Energy Inst. *90*, 902–913. https://doi.org/10.1016/j.joei.2016.08.004.
19. Yang, H., Yan, R., Chen, H., Lee, D.H., and Zheng, C. (2007). Characteristics of hemicellulose, cellulose and lignin pyrolysis. Fuel *86*, 1781–1788. https://doi.org/10.1016/j.fuel.2006.12.013.
20. Basu, P. (2018). Pyrolysis. In Biomass Gasification, Pyrolysis and Torrefaction (Elsevier), pp. 155–187. https://doi.org/10.1016/B978-0-12-812992-0.00005-4.
21. Sadakata, M., Takahashi, K., Saito, M., and Sakai, T. (1987). Production of fuel gas and char from wood, lignin and holocellulose by carbonization. Fuel *66*, 1667–1671. https://doi.org/10.1016/0016-2361(87)90360-7.
22. Sharma, R.K., Wooten, J.B., Baliga, V.L., Lin, X., Geoffrey Chan, W., and Hajaligol, M.R. (2004). Characterization of chars from pyrolysis of lignin. Fuel *83*, 1469–1482. https://doi.org/10.1016/j.fuel.2003.11.015.
23. Bourke, J., Manley-Harris, M., Fushimi, C., Dowaki, K., Nunoura, T., and Antal, M.J. (2007). Do All Carbonized Charcoals Have the Same Chemical Structure? 2. A Model of the Chemical Structure of Carbonized Charcoal. Ind. Eng. Chem. Res. *46*, 5954–5967. https://doi.org/10.1021/ie070415u.
24. Bajpai, P. (2022). Physical and chemical characteristics of lignocellulosic biomass. Lignocellul. Biomass Biotechnol. 11–24. https://doi.org/10.1016/B978-0-12-821889-1.00001-1.
25. Janu, R., Mrlik, V., Ribitsch, D., Hofman, J., Sedláček, P., Bielská, L., and Soja, G. (2021). Biochar surface functional groups as affected by biomass feedstock, biochar composition

and pyrolysis temperature. Carbon Resour. Convers. *4*, 36–46. https://doi.org/10.1016/j.crcon.2021.01.003.

26. Enders, A., Hanley, K., Whitman, T., Joseph, S., and Lehmann, J. (2012). Characterization of biochars to evaluate recalcitrance and agronomic performance. Bioresour. Technol. *114*, 644–653. https://doi.org/10.1016/j.biortech.2012.03.022.

27. Zhao, L., Cao, X., Mašek, O., and Zimmerman, A. (2013). Heterogeneity of biochar properties as a function of feedstock sources and production temperatures. J. Hazard Mater. *256–257*, 1–9. https://doi.org/10.1016/j.jhazmat.2013.04.015.

28. Mašek, O., Buss, W., Roy-Poirier, A., Lowe, W., Peters, C., Brownsort, P., Mignard, D., Pritchard, C., and Sohi, S. (2018). Consistency of biochar properties over time and production scales: A characterisation of standard materials. J. Anal. Appl. Pyrolysis *132*, 200–210. https://doi.org/10.1016/j.jaap.2018.02.020.

29. Mészáros, E., Jakab, E., Várhegyi, G., Bourke, J., Manley-Harris, M., Nunoura, T., and Antal, M.J. (2007). Do All Carbonized Charcoals Have the Same Chemical Structure? 1. Implications of Thermogravimetry−Mass Spectrometry Measurements. Ind. Eng. Chem. Res. *46*, 5943–5953. https://doi.org/10.1021/ie0615842.

30. Phounglamcheik, A., Wang, L., Romar, H., Kienzl, N., Broström, M., Ramser, K., Skreiberg, Ø., and Umeki, K. (2020). Effects of Pyrolysis Conditions and Feedstocks on the Properties and Gasification Reactivity of Charcoal from Woodchips. Energy Fuels *34*, 8353–8365. https://doi.org/10.1021/acs.energyfuels.0c00592.

31. Collard, F.X., and Blin, J. (2014). A Review on Pyrolysis of Biomass Constituents: Mechanisms and Composition of the Products Obtained from the Conversion of Cellulose, Hemicelluloses and Lignin at (Elsevier Ltd). https://doi.org/10.1016/j.rser.2014.06.013.

32. Ahmad, M., Rajapaksha, A.U., Lim, J.E., Zhang, M., Bolan, N., Mohan, D., Vithanage, M., Lee, S.S., and Ok, Y.S. (2014). Biochar as a sorbent for contaminant management in soil and water: A review. Chemosphere *99*, 19–33. https://doi.org/10.1016/j.chemosphere.2013.10.071.

33. ASTM D 1762-84 (2011). Standard Test Method for Chemical Analysis of Wood Charcoal. ASTM Int. *84*, 1–2.

34. Brewer, C.E., Schmidt-Rohr, K., Satrio, J.A., and Brown, R.C. (2009). Characterization of biochar from fast pyrolysis and gasification systems. Environ. Prog. Sustain. Energy *28*, 386–396. https://doi.org/10.1002/ep.10378.

35. Illingworth, J., Williams, P.T., and Rand, B. (2013). Characterisation of biochar porosity from pyrolysis of biomass flax fibre. J. Energy Inst. *86*, 63–70. https://doi.org/10.1179/1743967112Z.00000000046.

36. Singh, B., Camps-Arbestain, M., and Lehmann, J.; CSIRO (Australia (2017). Biochar: A Guide to Analytical Methods.

37. Nzihou, A. (2020). Handbook on Characterization of Biomass, Biowaste and Related By-Products A. Nzihou (Springer International Publishing). https://doi.org/10.1007/978-3-030-35020-8.

38. Solar, J., Hippe, F., Babich, A., Caballero, B.M., De Marco Rodríguez, I., Barriocanal, C., López-Urionabarrenechea, A., and Acha, E. (2021). Conversion of Injected Forestry Waste Biomass Charcoal in a Blast Furnace: Influence of Pyrolysis Temperature. Energy Fuels *35*, 529–538. https://doi.org/10.1021/acs.energyfuels.0c03040.

39. Pereira, R.C., Arbestain, M.C., Sueiro, M.V., and Maclá-Agulló, J.A. (2015). Assessment of the surface chemistry of wood-derived biochars using wet chemistry, Fourier transform infrared spectroscopy and X-ray photoelectron spectroscopy. Soil Res. *53*, 753–762. https://doi.org/10.1071/SR14194.

40. Calvelo Pereira, R., Kaal, J., Camps Arbestain, M., Pardo Lorenzo, R., Aitkenhead, W., Hedley, M., Macías, F., Hindmarsh, J., and Maciá-Agulló, J.A. (2011). Contribution to characterisation of biochar to estimate the labile fraction of carbon. Org. Geochem. *42*, 1331–1342. https://doi.org/10.1016/j.orggeochem.2011.09.002.

41. Vassilev, S.V., Baxter, D., Andersen, L.K., and Vassileva, C.G. (2013). An Overview of the Composition and Application of Biomass Ash. Part 1. Phase-Mineral and Chemical Composition and Classification at (Elsevier). https://doi.org/10.1016/j.fuel.2012.09.041.

42. Banik, C., Lawrinenko, M., Bakshi, S., and Laird, D.A. (2018). Impact of Pyrolysis Temperature and Feedstock on Surface Charge and Functional Group Chemistry of Biochars. J. Environ. Qual. *47*, 452–461. https://doi.org/10.2134/jeq2017.11.0432.

43. Lü, J., Li, J., Li, Y., Chen, B., and Bao, Z. (2012). Use of rice straw biochar simultaneously as the sustained release carrier of herbicides and soil amendment for their reduced leaching. J. Agric. Food Chem. *60*, 6463–6470. https://doi.org/10.1021/jf3009734.

44. Brewer, C.E., Chuang, V.J., Masiello, C.A., Gonnermann, H., Gao, X., Dugan, B., Driver, L.E., Panzacchi, P., Zygourakis, K., and Davies, C.A. (2014). New approaches to measuring biochar density and porosity. Biomass Bioenergy *66*, 176–185. https://doi.org/10.1016/j.biombioe.2014.03.059.

45. Wang, P., Zhang, J., Shao, Q., and Wang, G. (2018). Physicochemical properties evolution of chars from palm kernel shell pyrolysis. J. Therm. Anal. Calorim. *133*, 1271–1280. https://doi.org/10.1007/s10973-018-7185-z.

46. Pusceddu, E., Santilli, S.F., Fioravanti, G., Montanaro, A., Miglietta, F., and Foscolo, P.U. (2019). Chemical-physical analysis and exfoliation of biochar-carbon matter: From agriculture soil improver to starting material for advanced nanotechnologies. Mater. Res. Express *6*, 115612. https://doi.org/10.1088/2053-1591/ab4ba8.

47. Xiao, X., and Chen, B. (2017). A Direct Observation of the Fine Aromatic Clusters and Molecular Structures of Biochars. Environ. Sci. Technol. *51*, 5473–5482. https://doi.org/10.1021/acs.est.6b06300.

48. Brown, R.A., Kercher, A.K., Nguyen, T.H., Nagle, D.C., and Ball, W.P. (2006). Production and characterization of synthetic wood chars for use as surrogates for natural sorbents. Org. Geochem. *37*, 321–333. https://doi.org/10.1016/j.orggeochem.2005.10.008.

49. Zhao, S.X., Ta, N., and Wang, X.D. (2017). Effect of temperature on the structural and physicochemical properties of biochar with apple tree branches as feedstock material. Energies *10*, 1293. https://doi.org/10.3390/en10091293.

50. Schneider, M.P., Hilf, M., Vogt, U.F., and Schmidt, M.W. (2010). The benzene polycarboxylic acid (BPCA) pattern of wood pyrolyzed between 200°C and 1000°C. Org. Geochem. *41*, 1082–1088. https://doi.org/10.1016/j.orggeochem.2010.07.001.

51. Koch, B.P., and Dittmar, T. (2006). From mass to structure: an aromaticity index for high-resolution mass data of natural organic matter. Rapid Commun. Mass Spectrom. *20*, 926–932. https://doi.org/10.1002/rcm.2386.

52. Xiao, X., Chen, Z., and Chen, B. (2016). H/C atomic ratio as a smart linkage between pyrolytic temperatures, aromatic clusters and sorption properties of biochars derived from diverse precursory materials. Sci. Rep. *6*, 22644. https://doi.org/10.1038/srep22644.

53. de Tomas, C., Suarez-Martinez, I., and Marks, N.A. (2016). Graphitization of amorphous carbons: A comparative study of interatomic potentials. Carbon N. Y. *109*, 681–693. https://doi.org/10.1016/j.carbon.2016.08.024.

54. Franklin, R.E. (1951). Crystallite growth in graphitizing and non-graphitizing carbons. Proc. R. Soc. London. Ser. A. Math. Phys. Sci. *209*, 196–218. https://doi.org/10.1098/rspa.1951.0197.

55. Cohen-Ofri, I., Weiner, L., Boaretto, E., Mintz, G., and Weiner, S. (2006). Modern and fossil charcoal: Aspects of structure and diagenesis. J. Archaeol. Sci. *33*, 428–439. https://doi.org/10.1016/j.jas.2005.08.008.

56. McBeath, A.V., and Smernik, R.J. (2009). Variation in the degree of aromatic condensation of chars. Org. Geochem. *40*, 1161–1168. https://doi.org/10.1016/j.orggeochem.2009.09.006.

57. Smernik, R.J., Kookana, R.S., and Skjemstad, J.O. (2006). NMR characterization of 13C-benzene sorbed to natural and prepared charcoals. Environ. Sci. Technol. *40*, 1764–1769. https://doi.org/10.1021/es051895o.

58. McBeath, A.V., Smernik, R.J., Krull, E.S., and Lehmann, J. (2014). The influence of feedstock and production temperature on biochar carbon chemistry: A solid-state 13C NMR study. Biomass Bioenergy *60*, 121–129. https://doi.org/10.1016/j.biombioe.2013.11.002.

59. Wiedemeier, D.B., Abiven, S., Hockaday, W.C., Keiluweit, M., Kleber, M., Masiello, C.A., McBeath, A.V., Nico, P.S., Pyle, L.A., Schneider, M.P., et al. (2015). Aromaticity and degree of aromatic condensation of char. Org. Geochem. *78*, 135–143. https://doi.org/10.1016/j.orggeochem.2014.10.002.

60. McBeath, A.V., Smernik, R.J., Schneider, M.P., Schmidt, M.W., and Plant, E.L. (2011).

Determination of the aromaticity and the degree of aromatic condensation of a thermosequence of wood charcoal using NMR. Org. Geochem. *42*, 1194–1202. https://doi.org/10.1016/j.orggeochem.2011.08.008.

61. Kaal, J., Brodowski, S., Baldock, J.A., Nierop, K.G., and Cortizas, A.M. (2008). Characterisation of aged black carbon using pyrolysis-GC/MS, thermally assisted hydrolysis and methylation (THM), direct and cross-polarisation 13C nuclear magnetic resonance (DP/CP NMR) and the benzenepolycarboxylic acid (BPCA) method. Org. Geochem. *39*, 1415–1426. https://doi.org/10.1016/j.orggeochem.2008.06.011.

62. Glaser, B., Haumaier, L., Guggenberger, G., and Zech, W. (1998). Black carbon in soils: The use of benzenecarboxylic acids as specific markers. Org. Geochem. *29*, 811–819. https://doi.org/10.1016/S0146-6380(98)00194-6.

63. Brodowski, S., Rodionov, A., Haumaier, L., Glaser, B., and Amelung, W. (2005). Revised black carbon assessment using benzene polycarboxylic acids. Org. Geochem. *36*, 1299–1310. https://doi.org/10.1016/j.orggeochem.2005.03.011.

64. Vidal, J.L., Gallant, S.M.V., Connors, E.P., Richards, D.D., Macquarrie, S.L., and Kerton, F.M. (2021). Green Solvents for the Liquid-Phase Exfoliation of Biochars. ACS Sustain. Chem. Eng. *9*, 9114–9125. https://doi.org/10.1021/acssuschemeng.1c02823.

65. Cole, D.P., Smith, E.A., and Lee, Y.J. (2012). High-resolution mass spectrometric characterization of molecules on biochar from pyrolysis and gasification of switchgrass. In Energy and Fuels (American Chemical Society), pp. 3803–3809. https://doi.org/10.1021/ef300356u.

66. Martin, J.W., Nyadong, L., Ducati, C., Manley-Harris, M., Marshall, A.G., and Kraft, M. (2019). Nanostructure of Gasification Charcoal (Biochar). Environ. Sci. Technol. *53*, 3538–3546. https://doi.org/10.1021/acs.est.8b06861.

67. Zhao, N., Lv, Y., and Yang, X. (2017). A new 3D conceptual structure modeling of biochars by molecular mechanic and molecular dynamic simulation. J. Soils Sediments *17*, 641–655. https://doi.org/10.1007/s11368-015-1308-y.

68. McKenna, A.M., Chacón-Patiño, M.L., Chen, H., Blakney, G.T., Mentink-Vigier, F., Young, R.B., Ippolito, J.A., and Borch, T. (2021). Expanding the Analytical Window for Biochar Speciation: Molecular Comparison of Solvent Extraction and Water-Soluble Fractions of Biochar by FT-ICR Mass Spectrometry. Anal. Chem. *93*, 15365–15372. https://doi.org/10.1021/ACS.ANALCHEM.1C03058/ASSET/IMAGES/LARGE/AC1C03058_0005.JPEG.

69. Oberlin, A. (1984). Carbonization and graphitization. Carbon N. Y. *22*, 521–541. https://doi.org/10.1016/0008-6223(84)90086-1.

70. Harris, P.J.F. (2013). Fullerene-like models for microporous carbon. J. Mater. Sci. *48*, 565–577. https://doi.org/10.1007/s10853-012-6788-1.

71. Harris, P.J.F. (1997). Structure of non-graphitising carbons at. Int. Mater. Rev. *42*, 206–218. https://doi.org/10.1179/imr.1997.42.5.

72. Harris, P.J.F., Burian, A., and Duber, S. (2000). High-resolution electron microscopy of a microporous carbon. Phil. Mag. Lett. *80*, 381–386. https://doi.org/10.1080/095008300403512.

73. Guo, J., Morris, J.R., Ihm, Y., Contescu, C.I., Gallego, N.C., Duscher, G., Pennycook, S.J., and Chisholm, M.F. (2012). Topological Defects: Origin of Nanopores and Enhanced Adsorption Performance in Nanoporous Carbon. Small *8*, 3283–3288. https://doi.org/10.1002/smll.201200894.

74. McDonald-Wharry, J.S., Manley-Harris, M., and Pickering, K.L. (2016). Reviewing, Combining, and Updating the Models for the Nanostructure of Non-Graphitizing Carbons Produced from Oxygen-Containing Precursors at. Energy Fuels *30*, 7811–7826. https://doi.org/10.1021/acs.energyfuels.6b00917.

75. Martin, J.W., De Tomas, C., Suarez-Martinez, I., Kraft, M., and Marks, N.A. (2019). Topology of disordered 3D graphene networks. Phys. Rev. Lett. *123*, 116105. https://doi.org/10.1103/PhysRevLett.123.116105.

76. Smith, M.A., Foley, H.C., and Lobo, R.F. (2004). A simple model describes the PDF of a non-graphitizing carbon. Carbon N. Y. *42*, 2041–2048. https://doi.org/10.1016/j.carbon.2004.04.009.

77. McDonald-Wharry, J., Manley-Harris, M., and Pickering, K. (2015). A comparison of the charring and carbonisation of oxygen-rich precursors with the thermal reduction of graphene oxide. Philos. Mag. A *95*, 4054–4077. https://doi.org/10.1080/14786435.2015.1108525.

78. Sharma, S., Shyam Kumar, C.N., Korvink, J.G., and Kübel, C. (2018). Evolution of Glassy Carbon Microstructure: In Situ Transmission Electron Microscopy of the Pyrolysis Process. Sci. Rep. *8*, 16282. https://doi.org/10.1038/s41598-018-34644-9.

79. Harris, P.J.F., and Tsang, S.C. (1997). High-resolution electron microscopy studies of non- graphitizing carbons. Philos. Mag. A Phys. Condens. Matter, Struct. Defects Mech. Prop. *76*, 667–677. https://doi.org/10.1080/01418619708214028.

80. Harris, P.J.F. (2019). Non-graphitizing carbon: Its structure and formation from organic precursors. Eurasian Chem. J. *21*, 227. https://doi.org/10.18321/ectj863.

81. Vallejos-Burgos, F., Díaz-Pérez, N., Silva-Villalobos, Á., Jiménez, R., García, X., and Radovic, L.R. (2016). On the structural and reactivity differences between biomass- and coal-derived chars. Carbon N. Y. *109*, 253–263. https://doi.org/10.1016/j.carbon.2016.08.012.

82. Pulido-Novicio, L., Hata, T., Kurimoto, Y., Doi, S., Ishihara, S., and Imamura, Y. (2001). Adsorption capacities and related characteristics of wood charcoals carbonized using a one-step or two-step process. J. Wood Sci. *47*, 48–57. https://doi.org/10.1007/BF00776645.

83. Marriott, A.S., Hunt, A.J., Bergström, E., Wilson, K., Budarin, V.L., Thomas-Oates, J., Clark, J.H., and Brydson, R. (2014). Investigating the structure of biomass-derived non-graphitizing mesoporous carbons by electron energy loss spectroscopy in the transmission electron microscope and X-ray photoelectron spectroscopy. Carbon N. Y. *67*, 514–524. https://doi.org/10.1016/j.carbon.2013.10.024.

84. Deldicque, D., Rouzaud, J.N., and Velde, B. (2016). A Raman - HRTEM study of the carbonization of wood: A new Raman-based paleothermometer dedicated to archaeometry. Carbon N. Y. *102*, 319–329. https://doi.org/10.1016/j.carbon.2016.02.042.

85. Rouzaud, J.N., Deldicque, D., Charon, É., and Pageot, J. (2015). Carbons at the heart of questions on energy and environment: A nanostructural approach. Compt. Rendus Geosci. *347*, 124–133. https://doi.org/10.1016/j.crte.2015.04.004.

86. Koo-amornpattana, W., Jonglertjunya, W., Phadungbut, P., Ratchahat, S., Kunthakudee, N., Chalermsinsuwan, B., and Hunsom, M. (2022). Valorization of spent disposable wooden chopstick as the CO2 adsorbent for a CO2/H2 mixed gas purification. Sci. Rep. *121*, 6250–6316. https://doi.org/10.1038/s41598-022-10197-w.

87. Matthews, M.J., Pimenta, M.A., Dresselhaus, G., Dresselhaus, M.S., and Endo, M. (1999). Origin of dispersive effects of the Raman D band in carbon materials. Phys. Rev. B *59*, R6585–R6588. https://doi.org/10.1103/physrevb.59.r6585.

88. Kelemen, S.R., and Fang, H.L. (2001). Maturity trends in Raman spectra from kerogen and coal. Energy Fuels *15*, 653–658. https://doi.org/10.1021/ef0002039.

89. Schito, A., Romano, C., Corrado, S., Grigo, D., and Poe, B. (2017). Diagenetic thermal evolution of organic matter by Raman spectroscopy. Org. Geochem. *106*, 57–67. https://doi.org/10.1016/j.orggeochem.2016.12.006.

90. Sadezky, A., Muckenhuber, H., Grothe, H., Niessner, R., and Pöschl, U. (2005). Raman microspectroscopy of soot and related carbonaceous materials: Spectral analysis and structural information. Carbon N. Y. *43*, 1731–1742. https://doi.org/10.1016/J.CARBON.2005.02.018.

91. Smith, M.W., Dallmeyer, I., Johnson, T.J., Brauer, C.S., McEwen, J.S., Espinal, J.F., and Garcia-Perez, M. (2016). Structural analysis of char by Raman spectroscopy: Improving band assignments through computational calculations from first principles. Carbon N. Y. *100*, 678–692. https://doi.org/10.1016/j.carbon.2016.01.031.

92. Mukome, F.N.D., Zhang, X., Silva, L.C.R., Six, J., and Parikh, S.J. (2013). Use of chemical and physical characteristics to investigate trends in biochar feedstocks. J. Agric. Food Chem. *61*, 2196–2204. https://doi.org/10.1021/jf3049142.

93. Ocampo-Perez, R., Padilla-Ortega, E., Medellin-Castillo, N.A., Coronado-Oyarvide, P., Aguilar-Madera, C.G., Segovia-Sandoval,

S.J., Flores-Ramírez, R., and Parra-Marfil, A. (2019). Synthesis of biochar from chili seeds and its application to remove ibuprofen from water. Equilibrium and 3D modeling. Sci. Total Environ. *655*, 1397–1408. https://doi.org/10.1016/j.scitotenv.2018.11.283.

94. Tuinstra, F., and Koenig, J.L. (1970). Raman Spectrum of Graphite. J. Chem. Phys. *53*, 1126–1130. https://doi.org/10.1063/1.1674108.

95. Wopenka, B., and Pasteris, J.D. (1993). Structural characterization of kerogens to granulite-facies graphite: applicability of Raman microprobe spectroscopy. Am. Mineral. *78*, 533–557.

96. Keiluweit, M., Nico, P.S., Johnson, M.G., and Kleber, M. (2010). Dynamic molecular structure of plant biomass-derived black carbon (biochar). Environ. Sci. Technol. *44*, 1247–1253. https://doi.org/10.1021/es9031419.

97. Cetin, E., Moghtaderi, B., Gupta, R., and Wall, T.F. (2004). Influence of pyrolysis conditions on the structure and gasification reactivity of biomass chars. Fuel *83*, 2139–2150. https://doi.org/10.1016/j.fuel.2004.05.008.

98. Mohanty, P., Nanda, S., Pant, K.K., Naik, S., Kozinski, J.A., and Dalai, A.K. (2013). Evaluation of the physiochemical development of biochars obtained from pyrolysis of wheat straw, timothy grass and pinewood: Effects of heating rate. J. Anal. Appl. Pyrolysis *104*, 485–493. https://doi.org/10.1016/J.JAAP.2013.05.022.

99. Bragg, W.L. (1913). The Diffraction of Short Electromagnetic Waves by a Crystal. In Proceedings of the Cambridge Philosophical Society, pp. 43–57.

100. Thomas, J.M. (2012). Centenary: The Birth of X-Ray Crystallography at (Nature Publishing Group). https://doi.org/10.1038/491186a.

101. Scherrer, P. (1912). Bestimmung der inneren Struktur und der Größe von Kolloidteilchen mittels Röntgenstrahlen (Kolloidchemie Ein Lehrbuch), pp. 387–409. https://doi.org/10.1007/978-3-662-33915-2_7.

102. Marsh, H., and Rodríguez-Reinoso, F. (2006). Activated Carbon (Elsevier Ltd). https://doi.org/10.1016/B978-0-08-044463-5.X5013-4.

103. Lim, D.J., Marks, N.A., and Rowles, M.R. (2020). Universal Scherrer equation for graphene fragments. Carbon N. Y. *162*, 475–480. https://doi.org/10.1016/J.CARBON.2020.02.064.

104. Putman, K.J., Rowles, M.R., Marks, N.A., Suarez-Martinez, I., Onuki, J., Isshiki -, M., Putman, K.J., Rowles, M.R., Marks, N.A., et al. (2021). The role of the 2D-to-3D transition in x-ray diffraction analysis of crystallite size. J. Phys. Condens. Matter *33*, 294002. https://doi.org/10.1088/1361-648X/AC0083.

105. Ban, L.L., Crawford, D., and Marsh, H. (1975). Lattice-resolution electron microscopy in structural studies of non-graphitizing carbons from polyvinylidene chloride (PVDC). J. Appl. Crystallogr. *8*, 415–420. https://doi.org/10.1107/s0021889875010904.

106. Rennhofer, H., Köhnke, J., Keckes, J., Tintner, J., Unterweger, C., Zinn, T., Deix, K., Lichtenegger, H., and Gindl-Altmutter, W. (2021). Pore Development during the Carbonization Process of Lignin Microparticles Investigated by Small Angle X-ray Scattering. Molecules *26*, 2087. https://doi.org/10.3390/molecules26072087.

107. Boehm, H.P. (1994). Some aspects of the surface chemistry of carbon blacks and other carbons. Carbon N. Y. *32*, 759–769. https://doi.org/10.1016/0008-6223(94)90031-0.

108. Boehm, H.-P., Diehl, E., Heck, W., and Sappok, R. (1964). Surface Oxides of Carbon. Angew. Chem., Int. Ed. Engl. *3*, 669–677. https://doi.org/10.1002/anie.196406691.

109. Boehm, H.P. (2002). Surface oxides on carbon and their analysis: A critical assessment. Carbon N. Y. *40*, 145–149. https://doi.org/10.1016/S0008-6223(01)00165-8.

110. Askeland, M., Clarke, B., and Paz-Ferreiro, J. (2019). Comparative characterization of biochars produced at three selected pyrolysis temperatures from common woody and herbaceous waste streams. PeerJ *7*, e6784. https://doi.org/10.7717/peerj.6784.

111. Chandra, S., and Bhattacharya, J. (2019). Influence of temperature and duration of pyrolysis on the property heterogeneity of rice straw biochar and optimization of pyrolysis conditions for its application in soils. J. Clean. Prod. *215*, 1123–1139. https://doi.org/10.1016/j.jclepro.2019.01.079.

112. Kirtania, K., Tanner, J., Kabir, K.B., Rajendran, S., and Bhattacharya, S. (2014). In situ synchrotron IR study relating temperature and heating rate to surface functional group changes in biomass. Bioresour. Technol. *151*, 36–42. https://doi.org/10.1016/j.biortech.2013.10.034.

113. Li, B., Liu, D., Lin, D., Xie, X., Wang, S., Xu, H., Wang, J., Huang, Y., Zhang, S., and Hu, X. (2020). Changes in Biochar Functional Groups and Its Reactivity after Volatile-Char Interactions during Biomass Pyrolysis. Energy Fuels *34*, 14291–14299. https://doi.org/10.1021/acs.energyfuels.0c03243.

114. Trivedi, N.S., Mandavgane, S.A., and Chaurasia, A. (2018). Characterization and valorization of biomass char: a comparison with biomass ash. Environ. Sci. Pollut. Res. Int. *25*, 3458–3467. https://doi.org/10.1007/s11356-017-0689-4.

115. Paul, D., Kasera, N., Kolar, P., and Hall, S.G. (2020). Physicochemical characterization data of pine-derived biochar and natural zeolite as precursors to catalysts. Chem. Data Collect. *30*, 100573. https://doi.org/10.1016/j.cdc.2020.100573.

116. Leng, L., Liu, R., Xu, S., Mohamed, B.A., Yang, Z., Hu, Y., Chen, J., Zhao, S., Wu, Z., Peng, H., et al. (2022). An Overview of Sulfur-Functional Groups in Biochar from Pyrolysis of Biomass at (Elsevier). https://doi.org/10.1016/j.jece.2022.107185.

117. Perry, D.L., and Grint, A. (1983). Application of XPS to coal characterization. Fuel *62*, 1024–1033. https://doi.org/10.1016/0016-2361(83)90135-7.

118. Suliman, W., Harsh, J.B., Abu-Lail, N.I., Fortuna, A.M., Dallmeyer, I., and Garcia-Perez, M. (2016). Modification of biochar surface by air oxidation: Role of pyrolysis temperature. Biomass Bioenergy *85*, 1–11. https://doi.org/10.1016/j.biombioe.2015.11.030.

119. Leng, L., Xu, S., Liu, R., Yu, T., Zhuo, X., Leng, S., Xiong, Q., and Huang, H. (2020). Nitrogen Containing Functional Groups of Biochar: An Overview at (Elsevier). https://doi.org/10.1016/j.biortech.2019.122286.

120. Suliman, W., Harsh, J.B., Abu-Lail, N.I., Fortuna, A.M., Dallmeyer, I., and Garcia-Pérez, M. (2017). The role of biochar porosity and surface functionality in augmenting hydrologic properties of a sandy soil. Sci. Total Environ. *574*, 139–147. https://doi.org/10.1016/j.scitotenv.2016.09.025.

121. Li, N., Ma, X., Zha, Q., Kim, K., Chen, Y., and Song, C. (2011). Maximizing the number of oxygen-containing functional groups on activated carbon by using ammonium persulfate and improving the temperature-programmed desorption characterization of carbon surface chemistry. Carbon N. Y. *49*, 5002–5013. https://doi.org/10.1016/J.CARBON.2011.07.015.

122. de la Puente, G., Pis, J.J., Menéndez, J.A., and Grange, P. (1997). Thermal stability of oxygenated functions in activated carbons. J. Anal. Appl. Pyrolysis *43*, 125–138. https://doi.org/10.1016/S0165-2370(97)00060-0.

123. Otake, Y., and Jenkins, R.G. (1993). Characterization of oxygen-containing surface complexes created on a microporous carbon by air and nitric acid treatment. Carbon N. Y. *31*, 109–121. https://doi.org/10.1016/0008-6223(93)90163-5.

124. Zhuang, Q.L., Kyotani, T., and Tomita, A. (1994). DRIFT and TK/TPD Analyses of Surface Oxygen Complexes Formed during Carbon Gasification. Energy Fuels *8*, 714–718. https://doi.org/10.1021/EF00045A028/ASSET/EF00045A028.FP.PNG_V03.

125. Zielke, U., Hüttinger, K.J., and Hoffman, W.P. (1996). Surface-oxidized carbon fibers: I. Surface structure and chemistry. Carbon N. Y. *34*, 983–998. https://doi.org/10.1016/0008-6223(96)00032-2.

126. Marchon, B., Carrazza, J., Heinemann, H., and Somorjai, G.A. (1988). TPD and XPS studies of O2, CO2, and H2O adsorption on clean polycrystalline graphite. Carbon N. Y. *26*, 507–514. https://doi.org/10.1016/0008-6223(88)90149-2.

127. Figueiredo, J.L., Pereira, M.F.R., Freitas, M.M.A., and Órfão, J.J.M. (1999). Modification of the surface chemistry of activated carbons. Carbon N. Y. *37*, 1379–1389. https://doi.org/10.1016/S0008-6223(98)00333-9.

128. Samant, P.V., Gonçalves, F., Freitas, M.M.A., Pereira, M.F.R., and Figueiredo, J.L. (2004). Surface activation of a polymer based carbon. In Carbon (Pergamon), pp. 1321–1325. https://doi.org/10.1016/j.carbon.2004.01.034.

129. Figueiredo, J.L., and Pereira, M.F.R. (2010). The role of surface chemistry in catalysis with carbons. Catal. Today *150*, 2–7. https://doi.org/10.1016/J.CATTOD.2009.04.010.

130. Fan, M., Li, C., Sun, Y., Zhang, L., Zhang, S., and Hu, X. (2021). In situ characterization of functional groups of biochar in pyrolysis of cellulose. Sci. Total Environ. *799*, 149354. https://doi.org/10.1016/j.scitotenv.2021.149354.

131. Reeves, J.B. (2012). Mid-Infrared Spectroscopy of Biochars and Spectral Similarities to Coal and Kerogens: What Are the Implications? Appl. Spectrosc. *66*, 689–695. https://doi.org/10.1366/11-06478.

132. Sbizzaro, M., César Sampaio, S., Rinaldo dos Reis, R., de Assis Beraldi, F., Medina Rosa, D., Maria Branco de Freitas Maia, C., Saramago de Carvalho Marques dos Santos Cordovil, C., Tillvitz do Nascimento, C., Antonio da Silva, E., and Eduardo Borba, C. (2021). Effect of production temperature in biochar properties from bamboo culm and its influences on atrazine adsorption from aqueous systems. J. Mol. Liq. *343*, 117667. https://doi.org/10.1016/j.molliq.2021.117667.

133. Chen, Z., Xiao, X., Chen, B., and Zhu, L. (2015). Quantification of chemical states, dissociation constants and contents of oxygen-containing groups on the surface of biochars produced at different temperatures. Environ. Sci. Technol. *49*, 309–317. https://doi.org/10.1021/es5043468.

134. Li, Z.Q., Lu, C.J., Xia, Z.P., Zhou, Y., and Luo, Z. (2007). X-ray diffraction patterns of graphite and turbostratic carbon. Carbon N. Y. *45*, 1686–1695. https://doi.org/10.1016/j.carbon.2007.03.038.

135. Felts, J.R., Oyer, A.J., Hernández, S.C., Whitener, K.E., Robinson, J.T., Walton, S.G., and Sheehan, P.E. (2015). Direct mechanochemical cleavage of functional groups from graphene. Nat. Commun. *61*, 1–7. https://doi.org/10.1038/ncomms7467.

136. Chang, D.W., Choi, H.J., Jeon, I.Y., Seo, J.M., Dai, L., and Baek, J.B. (2014). Solvent-free mechanochemical reduction of graphene oxide. Carbon N. Y. *77*, 501–507. https://doi.org/10.1016/J.CARBON.2014.05.055.

137. Burk, L., Gliem, M., Mülhaupt, R., Burk, L., Gliem, M., and Mülhaupt, R. (2019). Mechanochemical Routes to Functionalized Graphene Nanofillers Tuned for Lightweight Carbon/Hydrocarbon Composites. Macromol. Mater. Eng. *304*, 1800496. https://doi.org/10.1002/MAME.201800496.

138. Usman, A.R., Abduljabbar, A., Vithanage, M., Ok, Y.S., Ahmad, M., Ahmad, M., Elfaki, J., Abdulazeem, S.S., and Al-Wabel, M.I. (2015). Biochar production from date palm waste: Charring temperature induced changes in composition and surface chemistry. J. Anal. Appl. Pyrolysis *115*, 392–400. https://doi.org/10.1016/j.jaap.2015.08.016.

139. Baltrenas, P., Baltrenaite, E., and Spudulis, E. (2015). Biochar from pine and birch morphology and pore structure change by treatment in biofilter. Water Air Soil Pollut. *226*, 1–14. https://doi.org/10.1007/s11270-015-2295-8.

140. De Boer, J.H., and Steggerda, J. (1958). The helium density of micro-porous solids. In Proceedings of the Koninklijke Nederlandse Akademie van Wetenschappen. Series B, Palaeontology, geology, physics and chemistry (Koninklijke Nederlandse akademie van wetenschappen), pp. 318–323.

141. Kini, K.A., and Stacy, W.O. (1963). The adsorption of helium by carbonaceous solids. Carbon N. Y. *1*, 17–24. https://doi.org/10.1016/0008-6223(63)90005-8.

142. Menon, P.G. (1968). Adsorption at high pressures. Chem. Rev. *68*, 277–294. https://doi.org/10.1021/cr60253a002.

143. Greyson, J., and Aston, J.G. (1957). The heats of adsorption of helium and neon on graphitized carbon black. J. Phys. Chem. *61*, 610–613. https://doi.org/10.1021/j150551a021.

144. Maggs, F.A.P., Schwabe, P.H., and Williams, J.H. (1960). Adsorption of helium on carbons: Influence on measurement of density. Nature *186*, 956–958. https://doi.org/10.1038/186956b0.

145. Nguyen, H.G.T., Horn, J.C., Bleakney, M., Siderius, D.W., and Espinal, L. (2019). Understanding material characteristics through signature traits from helium pycnometry. Langmuir *35*, 2115–2122. https://doi.org/10.1021/acs.langmuir.8b03731.

146. Somerville, M., and Jahanshahi, S. (2015). The effect of temperature and compression during pyrolysis on the density of charcoal made from Australian eucalypt wood. Renew. Energy *80*, 471–478. https://doi.org/10.1016/j.renene.2015.02.013.

147. Giesche, H. (2006). Mercury Porosimetry: A General (Practical) Overview. Part. Part. Syst. Char. *23*, 9–19. https://doi.org/10.1002/PPSC.200601009.

148. Thommes, M., Kaneko, K., Neimark, A.V., Olivier, J.P., Rodriguez-Reinoso, F., Rouquerol, J., and Sing, K.S. (2015). Physisorption of gases, with special reference to the evaluation of surface area and pore size distribution (IUPAC Technical Report). Pure Appl. Chem. *87*, 1051–1069. https://doi.org/10.1515/pac-2014-1117.

149. Maziarka, P., Wurzer, C., Arauzo, P.J., Dieguez-Alonso, A., Mašek, O., and Ronsse, F. (2021). Do you BET on routine? The reliability of N2 physisorption for the quantitative assessment of biochar's surface area. Chem. Eng. J. *418*, 129234. https://doi.org/10.1016/j.cej.2021.129234.

150. Roussel, T., Jagiello, J., Pellenq, R.J.M., Thommes, M., and Bichara, C. (2006). Testing the feasibility of using the density functional theory route for pore size distribution calculations of ordered microporous carbons. Mol. Simulat. *32*, 551–555. https://doi.org/10.1080/08927020500517231.

151. Sigmund, G., Hüffer, T., Hofmann, T., and Kah, M. (2017). Biochar total surface area and total pore volume determined by N2 and CO2 physisorption are strongly influenced by degassing temperature. Sci. Total Environ. *580*, 770–775. https://doi.org/10.1016/J.SCITOTENV.2016.12.023.

152. Cheng, D., Ngo, H.H., Guo, W., Chang, S.W., Nguyen, D.D., Zhang, X., Varjani, S., and Liu, Y. (2020). Feasibility study on a new pomelo peel derived biochar for tetracycline antibiotics removal in swine wastewater. Sci. Total Environ. *720*, 137662. https://doi.org/10.1016/j.scitotenv.2020.137662.

153. Brewer, C.E., Unger, R., Schmidt-Rohr, K., and Brown, R.C. (2011). Criteria to Select Biochars for Field Studies based on Biochar Chemical Properties. Bioenergy Res. *4*, 312–323. https://doi.org/10.1007/s12155-011-9133-7.

154. Schlumberger, C., Scherdel, C., Kriesten, M., Leicht, P., Keilbach, A., Ehmann, H., Kotnik, P., Reichenauer, G., and Thommes, M. (2022). Reliable surface area determination of powders and meso/macroporous materials: Small-angle X-ray scattering and gas physisorption. Microporous Mesoporous Mater. *329*, 111554. https://doi.org/10.1016/j.micromeso.2021.111554.

155. Rouquerol, J., Llewellyn, P., and Rouquerol, F. (2007). Is the BET equation applicable to microporous adsorbents? Stud. Surf. Sci. Catal. *160*, 49–56. https://doi.org/10.1016/s0167-2991(07)80008-5.

156. Sigmund, G., Sun, H., Hofmann, T., and Kah, M. (2016). Predicting the Sorption of Aromatic Acids to Noncarbonized and Carbonized Sorbents. Environ. Sci. Technol. *50*, 3641–3648. https://doi.org/10.1021/acs.est.5b06033.

157. Břendová, K., Száková, J., Lhotka, M., Krulikovská, T., Punčochář, M., and Tlustoš, P. (2017). Biochar physicochemical parameters as a result of feedstock material and pyrolysis temperature: predictable for the fate of biochar in soil? Environ. Geochem. Health *39*, 1381–1395. https://doi.org/10.1007/s10653-017-0004-9.

158. Kupgan, G., Liyana-Arachchi, T.P., and Colina, C.M. (2017). NLDFT Pore Size Distribution in Amorphous Microporous Materials. Langmuir *33*, 11138–11145. https://doi.org/10.1021/acs.langmuir.7b01961.

159. Jagiello, J., Kenvin, J., Ania, C.O., Parra, J.B., Celzard, A., and Fierro, V. (2020). Exploiting the adsorption of simple gases O2 and H2 with minimal quadrupole moments for the dual gas characterization of nanoporous carbons using 2D-NLDFT models. Carbon N. Y. *160*, 164–175. https://doi.org/10.1016/J.CARBON.2020.01.013.

160. Villarroel-Rocha, J., Barrera, D., Arroyo-Gómez, J.J., and Sapag, K. (2021). Insights of adsorption isotherms with different gases at 77 K and their use to assess the BET area of nanoporous silica materials. Adsorption *27*,

1081–1093. https://doi.org/10.1007/S10450-021-00339-3/FIGURES/6.

161. Blankenship, L.S., Jagiello, J., and Mokaya, R. (2022). Confirmation of pore formation mechanisms in biochars and activated carbons by dual isotherm analysis. Mater. Adv. *3*, 3961–3971. https://doi.org/10.1039/D2MA00141A.

162. UC Davis Biochar Database Home http://biochar.ucdavis.edu/.

163. UK Biochar Research Centre UKBRC Charchive. https://www.charchive.org/records.php.

164. Ippolito, J.A., Cui, L., Kammann, C., Wrage-Mönnig, N., Estavillo, J.M., Fuertes-Mendizabal, T., Cayuela, M.L., Sigua, G., Novak, J., Spokas, K., et al. (2020). Feedstock Choice, Pyrolysis Temperature and Type Influence Biochar Characteristics: A Comprehensive Meta-Data Analysis Review at (Springer Science and Business Media B.V). https://doi.org/10.1007/s42773-020-00067-x.

165. Wang, L., Ok, Y.S., Tsang, D.C.W., Alessi, D.S., Rinklebe, J., Wang, H., Mašek, O., Hou, R., O'Connor, D., and Hou, D. (2020). New Trends in Biochar Pyrolysis and Modification Strategies: Feedstock, Pyrolysis Conditions, Sustainability Concerns and Implications for Soil Amendment at Blackwell Publishing Ltd. https://doi.org/10.1111/sum.12592.